nature biomedical engineering

ARTICLES

https://doi.org/10.1038/s41551-020-00656-y

Check for updates

Lentiviral delivery of co-packaged *Cas9* mRNA and a *Vegfa*-targeting guide RNA prevents wet age-related macular degeneration in mice

Sikai Ling[1,9], Shiqi Yang[2,9], Xinde Hu[3], Di Yin[1], Yao Dai[1], Xiaoqing Qian[4], Dawei Wang[5], Xiaoyong Pan[6], Jiaxu Hong[7], Xiaodong Sun[2], Hui Yang[3], Soren Riis Paludan[8] and Yujia Cai[1]✉

Therapeutic genome editing requires effective and targeted delivery methods. The delivery of *Cas9* mRNA using adeno-associated viruses has led to potent in vivo therapeutic efficacy, but can cause sustained *Cas9* expression, anti-Cas9 immune responses and off-target edits. Lentiviral vectors have been engineered to deliver nucleases that are expressed transiently, but in vivo evidence of their biomedical efficacy is lacking. Here, we show that the lentiviral codelivery of *Streptococcus pyogenes Cas9* mRNA and expression cassettes that encode a guide RNA that targets vascular endothelial growth factor A (*Vegfa*) is efficacious in a mouse model of wet age-related macular degeneration induced by *Vegfa*. A single subretinal injection of engineered lentiviruses knocked out 44% of *Vegfa* in retinal pigment epithelium and reduced the area of choroidal neovascularization by 63% without inducing off-target edits or anti-Cas9 immune responses. Engineered lentiviruses for the transient expression of nucleases may form the basis of new treatments for retinal neovascular diseases.

CRISPR is a powerful genome-editing tool that has shown potential for curing genetic diseases, acquired diseases and infectious diseases[1–3]. CRISPR delivered by adeno-associated viruses (AAVs) has recently been approved for use in a clinical trial (NCT03872479) for the in vivo treatment of severe retinal dystrophy in Leber congenital amaurosis type 10. Despite the impressive progress, the targeted and efficacious delivery of the CRISPR nucleases and guide RNAs (gRNAs) remains a critical bottleneck in the application of CRISPR for gene therapy[4].

AAVs are the most frequently used vector for in vivo gene editing with CRISPR[5,6]. Although the efficiency is generally high, AAV delivery suffers from (1) the difficulty of delivering Sp*Cas9*–gRNA and base editors, owing to vector-size restrictions[7], (2) off-target effects, owing to prolonged Cas9 expression[8], (3) immune responses against Cas9 and the viral capsids[9,10] and (4) a high frequency of vector integrations in CRISPR-induced double-stranded breaks[11]. Recent studies have revealed widespread pre-existing immunity against Cas9 in the human population[12]. Although humoral immunity is most relevant for naked Cas9 proteins, Cas9 expressed from viral vectors is expected to result in the presentation of proteasome-spliced epitopes by human leukocyte antigen (HLA) class I, potentially attracting Cas9-specific cytotoxic T lymphocytes (CTLs)[13].

In the clinical scenario, transiently exposing Cas9 in the form of mRNA or recombinant protein is highly desired to ensure safety and long-term efficacy. In this regard, non-viral nanoparticles are attractive for CRISPR delivery. Lipid-based non-viral nanoparticles have been shown to deliver Cas9–gRNA ribonucleoprotein (RNP) in vivo to modify inner-ear hair cells; however, the low efficiency is a barrier for their clinical translation, as lipid nanoparticles tend to become trapped in endosomes[14]. CRISPR RNP delivery by vesicles coated with vesicular stomatitis virus G (VSV-G) is based on non-specific packaging and, therefore, cellular proteins or RNA may also be co-packaged[15]. Gold nanoparticles in complex with endosomal disruptive polymer have the ability to escape endosomes, and have been used for CRISPR RNP delivery to human blood progenitors as well as to mouse muscle and brain[16–18]. However, this type of nanomaterial can accumulate in the liver and spleen for more than two months and significantly change the pattern of gene expression in several pathways[19].

Owing to mechanisms acquired through natural evolution, lentiviruses have the ability to cross cell membranes, escape endosomes and pass through the nuclear membrane with high efficiency. To deliver nucleases for therapeutic purposes, lentiviruses must be engineered to prevent permanent gene integration into the human genome. Lentiviruses have been engineered to carry protein or mRNA[20]. However, progress has been slow owing to the structural conservation of lentiviruses; a small change might disturb one of the crucial steps in the virus life cycle (such as assembly, maturation, infection or reverse transcription[21,22]). Lentiviral particles have been engineered as carriers of proteins for the delivery of site-specific nucleases—including ZFN, TALEN and Cas9—in a 'hit and run' mode. However, these achieved only modest efficiency[23–25]. Recently, attempts have also been made to deliver the mRNA or protein of a short version of Cas9 (*Staphylococcus aureus* Cas9), but gene

[1]Key Laboratory of Systems Biomedicine (Ministry of Education), Shanghai Center for Systems Biomedicine, Shanghai Jiao Tong University, Shanghai, China. [2]Department of Ophthalmology, Shanghai General Hospital (Shanghai First People's Hospital), Shanghai Jiao Tong University School of Medicine, Shanghai, China. [3]Institute of Neuroscience, State Key Laboratory of Neuroscience, Key Laboratory of Primate Neurobiology, Shanghai Institutes for Biological Sciences, Chinese Academy of Sciences, Shanghai, China. [4]School of Biomedical Engineering, Shanghai Jiao Tong University, Shanghai, China. [5]National Research Center for Translational Medicine, Ruijin Hospital Affiliated to Shanghai Jiao Tong University School of Medicine, Shanghai, China. [6]Key Laboratory of System Control and Information Processing (Ministry of Education), Institute of Image Processing and Pattern Recognition, Shanghai Jiao Tong University, Shanghai, China. [7]Department of Ophthalmology and Vision Science, Shanghai Eye, Ear, Nose and Throat Hospital, Fudan University, Shanghai, China. [8]Department of Biomedicine, Aarhus University, Aarhus, Denmark. [9]These authors contributed equally: Sikai Ling, Shiqi Yang. ✉e-mail: yujia.cai@sjtu.edu.cn

editing was verified for only one endogenous site, and the editing efficiency in HEK293T cells was low[26,27]. Moreover, the gRNA had to be provided separately[26]. Similarly, virus-like particles derived from retroviral vectors have also been used to deliver proteins or mRNA encoding gene-modifying enzymes, such as Cre, in vitro[28,29]. When the engineered retroviral vector was used to deliver *Sp*Cas9 protein in vivo, the efficiency of gene editing was relatively low (10%) even in tyrosinemia mice in which the edited cells obtained a growth advantage[30]. Overall, the successes of engineered lentiviruses or retroviruses for transient nuclease delivery have been largely limited to in vitro conditions.

Age-related macular degeneration (AMD) is a major cause of visual loss worldwide, affecting 20% of the growing aged population[31]. Aberrant development of blood vessels is a hallmark of wet AMD (wAMD). The present first-line treatment for wAMD involves anti-VEGF reagents (such as ranibizumab, bevacizumab and aflibercept), for which repeated invasive injections, if not life-long injections, are necessary[32]. Frequent injections are expensive, inconvenient, and carry a risk factor of ocular hypertension and endophthalmitis[33]. An alternative would involve the overexpression of anti-VEGF agents from lentiviruses or AAVs[34,35]. In particular, lentiviruses have been used in mouse models and in a phase-I clinical trial to treat wAMD by overexpressing anti-angiogenic factors; however, among all of the participants, only one showed convincing evidence of anti-permeability activity[34,36]. These strategies are therefore at an early stage, and their long-term efficacy is unclear. Moreover, they may be affected by (1) drug resistance, which has been observed for other anti-VEGF agents, (2) pre-existing anti-AAV immunity, which is common among the population, (3) leakage of anti-VEGF agents in the bloodstream and (4) systemic inhibition of angiogenesis. CRISPR–Cas9 genome editing represents a potential 'once and for all' treatment for wAMD, and may avoid drug resistance. Attempts at using *Vegfa*-specific Cas9–gRNA RNPs have shown a reduction in the choroidal neovascularization (CNV) area, but the efficacy is restricted to the injected locus, rendering it impractical for use in a clinical trial[2]. Integration-defective lentiviral vectors (IDLVs) have been used to deliver CRISPR in vitro and in vivo; however, the therapeutic potential of IDLVs in a CNV model remains to be verified[37,38]. The subretinal delivery of CRISPR by AAVs or by integration-proficient lentiviruses can disrupt *Vegfa*[7,39,40]. However, such traditional vectors are accompanied by long-term Cas9 expression; such redundant nuclease activity is a risk factor for safety. Thus, a method that delivers Cas9 transiently and efficiently for wAMD gene therapy is needed.

In this Article, we report a lentiviral system that delivers mRNA that encodes one of the longest Cas9 proteins (*Sp*Cas9) and gRNA simultaneously—which we named mLP-CRISPR, where mLP indicates mRNA-carrying lentiviral particles—and show that it prevents the development of wAMD in a mouse model of laser-induced CNV. When injected subretinally, mLP-CRISPR shows high tissue specificity to retinal pigment epithelium (RPE) cells, which are the only source of VEGFA in the posterior part of the eyes in adults[41]. Moreover, mLP-CRISPR does not induce anti-Cas9 IgG in the bloodstream or T-cell infiltration in the eyes. With a single injection, mLP-CRISPR knocks out 44% of *Vegfa* genes in RPE, and reduces the laser-induced CNV area by 63% in the wAMD mouse model. This is achieved using hit-and-run gene editing, and without causing detectable off-target events. The mLP system could be extended to deliver mRNA encoding other types of Cas9 nucleases, base editors, prime editors and epigenome editors.

Results

Construction of a lentiviral system for efficient mRNA delivery. HIV-1 encapsidates its RNAs efficiently and specifically over cytoplasmic RNAs through interactions between the psi signal on the viral RNA and the nucleocapsid protein[42]. To deliver external mRNA with the HIV-1 originated lentiviral particle, we imitated this machinery by taking the advantage of lentiviral protein transduction technology and the strong interaction between the bacteriophage-derived MS2 coat (MS2C) protein and its recognizing stem loop (pac site)[43,44]. The lentiviral Gag–Pol backbone is highly sensitive to insertions of foreign proteins depending on the locus and the size[23,24]. To determine the optimal engineering for mRNA delivery, we inserted the MS2C protein either as a monomer (1×) or dimer (2×) at the N or C terminus of Gag–Pol (Fig. 1a). To release the MS2C from Gag–Pol polyprotein after viral maturation, we introduced an HIV-1 protease cleavage signal (SQNY/PIVQ) between the foreign and viral protein (Fig. 1a). Meanwhile, we also inserted a MS2 stem loop between the stop codon and poly(A) to enable specific mRNA encapsidation through binding to the MS2C protein (Fig. 1b). The engineered Gag–Pol- and mRNA-expressing constructs were cotransfected into HEK293T cells in the presence of a VSV-G-encoding plasmid to produce mRNA-carrying lentiviral particles (designated mLPs; Fig. 1c).

We compared all of the Gag–Pol modifications using GFP as a readout, and found that the modification of Gag–Pol with a monomer MS2C protein fused at the Gag–Pol N terminus (MS2M–Gag–Pol) generated GFP$^+$ cells most efficiently (Fig. 1d and Supplementary Fig. 1a). Interestingly, although lentiviral particles generated from C-terminally modified Gag–Pol (Gag–Pol–MS2M) were functional in delivering *GFP* mRNA, their p24 level was beyond detection, indicating that the fusion of MS2C at this position undermined the process of lentiviral maturation and therefore inhibited Gag–Pol cleavage by HIV protease (Supplementary Fig. 1b). Indeed, we found that producer cells that were treated with the HIV protease inhibitor saquinavir produced significantly less p24, suggesting that the Gag–Pol fusion may block p24 antibody recognition (Supplementary Fig. 1c). We also examined whether the MS2M-Gag–Pol and Gag–Pol–MS2M modifications interfered with the vector-transfer ability of the original Gag–Pol. In contrast to our previous findings with transposase[24,45], here we found that Gag–Pol–MS2M lost the vector-transfer function, whereas MS2M–Gag–Pol retained the vector-transfer ability (Supplementary Fig. 1d). This suggests that the consequences of Gag–Pol engineering on viral function also depend on the structure of the inserted protein rather than only on the insertion loci. We therefore chose the N-terminally MS2-monomer-modified MS2M–Gag–Pol MS2 for further study. As the copy number of the stem loop in the mRNA may also be vital for mRNA packaging, we compared 3×, 6× and 12× repeats side by side, and found that *GFP* mRNA transfer increased with the number of copies (Supplementary Fig. 1e). Considering that the increased number of repeats might decrease the plasmid stability and decrease the space for cargo, we chose the 6× stem loop repeats in combination with the N-terminally MS2C-monomer-modified Gag–Pol for the subsequent mLP study. To examine the specificity of the *GFP* mRNA packaging, we included non-MS2C Gag–Pol (wild-type Gag–Pol) as a control. Our data showed that *GFP* mRNA packaging to mLP is MS2C dependent (Fig. 1e). Moreover, successful delivery required VSV-G-mediated viral entry (Fig. 1e).

With the optimized system, the percentage of GFP$^+$ cells could reach nearly 100% using 30 µl ultracentrifuged supernatant (Fig. 1f). We next compared mLP with the well-characterized conventional lentiviral vector side by side. Notably, mLP delivered *GFP* at a greater efficiency compared with the lentiviral system in an unsaturated condition with the same amount of particles (p24; Fig. 1g). As the lentiviral particles are a mixture of empty and infectious particles, our results suggest that mLP-GFP contains a higher percentage of transducible particles compared with the lentiviral vector. Notably, the intensity of gene expression from mLP was significantly lower compared with the intensity of gene expression from the lentivirus (typically more than fifteenfold lower, depending on the amount of viral particles; Fig. 1h). This might be a disadvantage

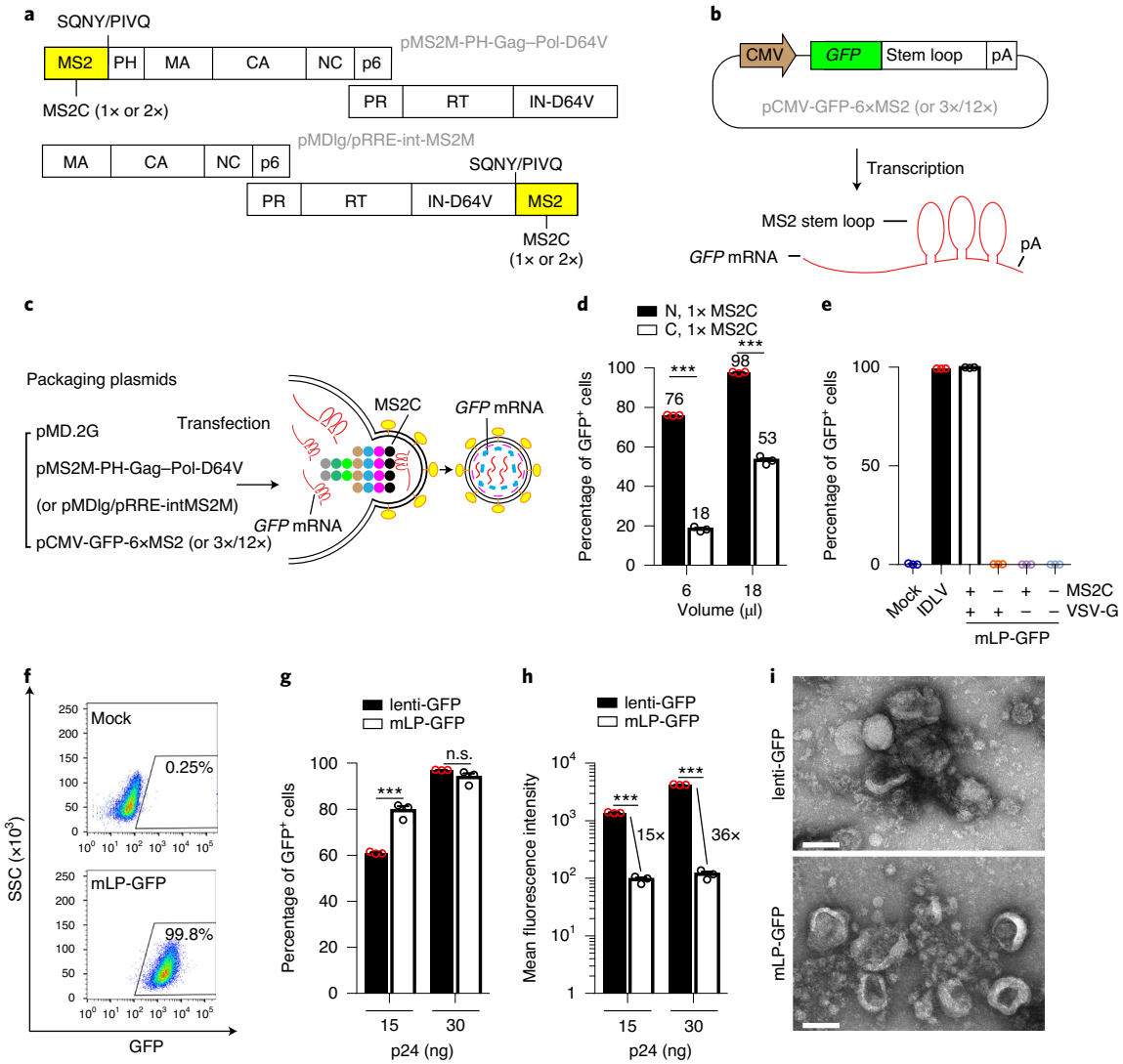

Fig. 1 | Construction of a lentiviral system for efficient mRNA delivery. a, The design of MS2C-modified lentiviral Gag–Pol polyprotein. The MS2C protein was fused to either the N terminus or the C terminus of Gag–Pol as a monomer (1×) or dimer (2×). SQNY/PIVQ is an HIV protease cleavage site. Gag is composed of a matrix (MA), capsid (CA) and nucleocapsid (NC), whereas Pol consists of a protease (PR), reverse transcriptase (RT) and integrase carrying a D64V mutation (IN^{D64V}). **b**, The design of the mRNA-encoding plasmid, which codes for the MS2-stem-loop-containing *GFP* mRNA. pA, poly(A). **c**, The principle of mLP-GFP production. **d**, Comparison of the efficiency of mRNA delivery. mLP-GFP was produced from Gag–Pol that was either N-terminally or C-terminally modified with a monomer MS2C in combination with 6× pac site repeats. ***$P < 0.0001$. **e**, The specificity of *GFP* mRNA packaging to mLP. Non-MS2C Gag–Pol (wild-type Gag–Pol) and VSV-G-negative mLP were used as controls. For each vector, 100 ng p24 was used. **f**, Representative flow cytometry analysis of GFP⁺ cells; 30 μl ultracentrifuged mLP-GFP, which was produced using the optimized production system, was used. **g**, Side-by-side comparison of the delivery efficiency between mLP-GFP and lenti-GFP. ***$P = 0.0008$ (15 ng p24 mLP-GFP versus lenti-GFP). **h**, Side-by-side comparison of the mean fluorescence intensity between mLP-GFP and lenti-GFP. ***$P < 0.0001$. **i**, Representative TEM images for mLP-GFP and lenti-GFP. Six images were taken for each group. Particles were visualized using uranyl acetate negative staining and imaged using a transmission electron microscope. Scale bars, 100 nm. Magnification, ×180,000. HEK293T cells were seeded 24 h before transduction at a density of 2×10^4 per well (**d**, **f**–**h**) or 4×10^4 per well (**e**). For **d**, **e**, **g** and **h**, data are mean ± s.e.m. from three biologically independent replicates. Statistical analysis was performed using unpaired two-tailed Student's *t*-tests.

for overexpression applications, but is an advantage for gene editing, as redundant Cas9 proteins increase the risk of off-target effects. Finally, we examined the morphologies of mLPs and lentiviruses using transmission electron microscopy (TEM). We found that mLPs and lentiviruses were indistinguishable in size and shape, suggesting that the viral structure was probably well maintained after Gag–Pol engineering (Fig. 1i).

mLP-Cas9 edits the genome through time-restricted nuclease exposure. To deliver *Cas9* mRNA using the mLP system, *Cas9* was inserted between the CMV promoter and the stem loop followed by a poly(A) sequence (Fig. 2a). To deliver gRNA, we inserted a U6-gRNA cassette into the U3 region of the self-inactivating third-generation lentiviral 3′ long terminal region (LTR). The resulting vector was combined with an integrase mutated (D64V) Gag–Pol to produce an IDLV such that the gRNA-expressing cassette would remain as a circular episome and not insert itself into the genome. The gRNA sequence in the 3′ LTR is copied to the 5′ LTR during reverse transcription; each viral episome will therefore have two copies of gRNA expression cassettes (Fig. 2b).

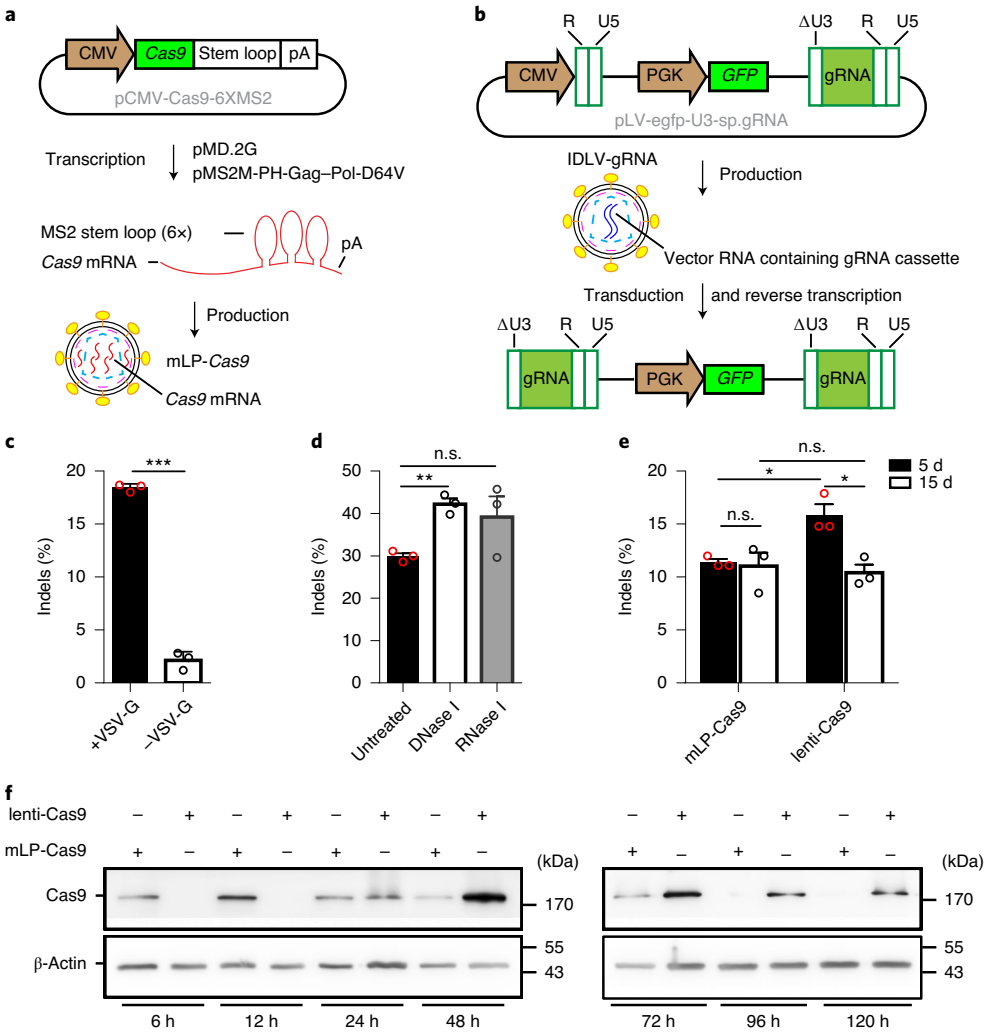

Fig. 2 | mLP-Cas9 edits genomes by time-restricted nuclease exposure. a, The principle of packaging *Cas9* mRNA into lentiviral particles to produce mLP-Cas9. **b**, Production and transduction of gRNA-expressing IDLV. gRNA was inserted into the U3 region of the 3′ LTR, which is copied to the 5′ LTR during reverse transcription. An integrase-mutated Gag–Pol was used to package the gRNA-expressing IDLV. R, a repeat region. **c**, Indels induced by VSV-G-coated and VSV-G-absent mLP-Cas9 (150 ng p24 for each). $^{***}P < 0.0001$. **d**, Gene editing by mLP-Cas9 pretreated with DNase I and RNase I. Untreated mLP-Cas9 was used as a control. $^{**}P = 0.0013$ (DNase-I treated versus untreated). For each vector, 250 ng p24. **e**, Long-term gene-editing effects by mLP-Cas9 and lenti-Cas9. The samples were collected 5 d and 15 d after transduction (150 ng p24) for analysis of indels. $^{*}P = 0.0134$ (lenti-Cas9 5 d versus 15 d); $^{*}P = 0.0146$ (lenti-Cas9 versus mLP-Cas9 on day 5). **f**, Western blot analysis of the lifespan of Cas9 protein after mLP and lentivirus delivery (150 ng p24). HEK293T cells that were seeded 24 h before transduction at a density of 2×10^4 per well were used for all of the experiments. gRNA was expressed from an *AAVS1*-targeting IDLV-gRNA (150 ng p24). For **c**–**e**, indel frequency was determined using Sanger sequencing and analysed using TIDE. Data are mean ± s.e.m. from three biologically independent replicates. Statistical analysis was performed using unpaired two-tailed Student's *t*-tests.

To verify whether the U6-gRNA cassette causes adverse effects on virus titres, we produced IDLVs using a transfer vector with or without a gRNA-coding cassette in the LTR, and compared their titres. As shown in Supplementary Fig. 2, we found no significant difference between the two groups, indicating that the U6-gRNA cassette in the LTR does not negatively affect virus yields. We first prepared mLP-Cas9 either in the presence or absence of a VSV-G envelope protein. Our results showed that mLP induced indels only in the presence of VSV-G, indicating that *Cas9* mRNA transfer depends on VSV-G-mediated endocytosis (Fig. 2c). To exclude the possibility that gene editing was mediated by plasmid or by mRNA carryover on the surface of lentiviral particles, the mLP-Cas9 was pretreated with DNase I and RNase I. After treatment, gene editing increased slightly due to growth inhibition induced by treatment (and therefore the higher multiplicity of infection for each cell), excluding the possibility of a surface carryover of nuclease (Fig. 2d).

We next compared the short-term and long-term gene-editing efficiencies of mLP-Cas9 and lenti-Cas9. The mLP-Cas9 was slightly less efficient compared with lenti-Cas9 on day 5; however, the efficiency was maintained over 15 d (Fig. 2e). By contrast, indel frequency in the lenti-Cas9 group was significantly reduced over time, consistent with our observations and previously published results that prolonged nuclease expression induces apoptosis[46] (Supplementary Fig. 3). To determine the exact lifespan of Cas9, the transduced cells were collected for western blot analysis at different time points. For lenti-Cas9, the Cas9 expression increased during the first 2 d, but decreased slightly after 120 h. Decreased gene expression is common for insertional lentiviruses owing to gene silencing; however, complete disappearance is unlikely[47]. To investigate

whether gene silencing caused a decrease in Cas9 expression from lenti-Cas9, we supplemented HEK293T cells with trichostatin A—an inhibitor of chromatin-remodelling histone deacetylases—during lenti-Cas9 transduction, and analysed Cas9 expression 120 h after transduction. As shown in Supplementary Fig. 4, treatment with trichostatin A efficiently enhanced the expression of Cas9 at two different concentrations, indicating that lenti-Cas9 was quickly silenced by transcriptional silencing. By contrast, Cas9 existed for only about 72 h after mLP mRNA transfer (Fig. 2f).

All-in-one mLP-CRISPR enhances gene-editing efficiency. An all-in-one CRISPR vector containing both *Cas9* and gRNA could potentially be more efficient for gene editing compared with the split form, whereby Cas9 and gRNA are provided from two different vectors as the latter needs two transduction events to complete gene editing. We therefore produced all-in-one CRISPR lentiviral particles (mLP-CRISPR) by integrating the mLP-Cas9 and IDLV-gRNA system by supplementing the mLP-Cas9 packaging system with three extra plasmids: pRSV-REV (encoding REV), pLV-egfp-U3-sp.gRNA (encoding GFP and gRNA) and pMDlg/pRRE-D64V (encoding wild-type but integrase-mutated Gag–Pol; Fig. 3a). The resultant all-in-one vector, mLP-Cas9 and IDLV-gRNA were individually transduced into HEK293T cells to verify the presence of *Cas9* mRNA and gRNA. We found that the presence of gRNA was consistently correlated with the presence of $Cas9^+$ cells, suggesting that the *Cas9* mRNA and gRNA were co-packaged in the same particle (Fig. 3b and Supplementary Fig. 5). Interestingly, the Cas9 signals were much stronger after all-in-one mLP-CRISPR delivery compared with after mLP-Cas9, although the former was supplemented with wild-type Gag–Pol, which in theory should dilute the number of mRNAs that a lentiviral particle can carry (Fig. 3b). Importantly, the conclusion was also replicable using western blot (Fig. 3c). These results together suggest that modifying viral Gag–Pol by N-terminally inserting an MS2C protein still impairs lentiviral function, which can be rescued by providing the wild-type Gag–Pol during the production process. To evaluate whether the specific interaction between the RNA stem loop and its cognate MS2C protein is necessary for efficient *Cas9* mRNA transfer, we produced mLP particles with or without MS2C, and in the presence or absence of gRNA. Although we observed MS2-independent delivery of *Cas9*, the presence of MS2C-containing Gag–Pol resulted in the delivery of twice as much *Cas9* (Supplementary Fig. 6).

Accordingly, the all-in-one mLP-CRISPR system was consistently more efficient at gene editing compared with the split counterpart at varying doses (Fig. 3d). We next compared mLP-CRISPR with the well-established lenti-CRISPR system, which is among the most efficient delivery systems[48]. We found that the gene editing by mLP was potent even at a low dose, although the conventional lentiviral vector was usually at least 39% more efficient than the nanoparticle when comparing at the same p24 level (Fig. 3e). Off-target effects are a major concern for CRISPR gene therapy. We therefore examined the off-targeting properties of *Cas9* mRNA delivery. We calculated the specificity score using the off-target/on-target ratio, and found that lenti-CRISPR scored 99.7 at off-target site OT2 and 65.6 at OT4; by contrast, at the same off-target sites, the specificity score for mLP-CRISPR was 12.6 and almost 0, respectively (Fig. 3f). These results indicate that gene editing using mLP is more precise compared with traditional long-term expression vectors, echoing previous observations[49]. To verify whether the mLP-CRISPR system can apply to difficult-to-transfect cell types, we tested the system in two suspension cell lines—K562 and Jurkat. In both cell lines, mLP-CRISPR induced about 60% indel frequency at the *AAVS1* locus (Fig. 3g).

It has been reported that the efficiency of CRISPR can be further improved by modifying the backbone of gRNA[50]. By combining with the optimized gRNA backbone, the gene-editing efficiency of mLP-CRISPR was indeed significantly higher in different cell lines and at different loci (Fig. 3h). To maximize gene editing in the subsequent in vivo study, we therefore chose the optimized gRNA backbone for *Vegfa*-targeting gRNA and verified it in vitro. In mouse embryonic fibroblasts (MEFs), mLP-CRISPR induced 43% indels at the *Vegfa* locus; in primary RPE cells, mLP-CRISPR induced 58% indels at the *Vegfa* locus (Fig. 3i). The varied efficiency of mLP-CRISPR in different cell types is probably a reflection of the cell transmissibility to the lentiviral particles, and the primary RPE cells are highly permissive for mLP-CRISPR.

To determine the copy number of *Cas9* mRNA per mLP particle, we used quantitative PCR with reverse transcription (RT–qPCR) to quantify the overall copies of *Cas9* mRNA normalized to lenti-CRISPR, which equips two copies of single-stranded *Cas9*-containing RNA per virion. The average copy number of *Cas9* mRNA in each mLP-CRISPR particle was about 3.5 consistently across different batches (Fig. 3j).

The innate immune response is detrimental to gene therapy. We therefore examined whether the engineered mRNA-carrying lentiviral particles induce type-I interferon (IFN) with the original lentiviral vectors as controls. We found that all of the vectors, including the mLP-Cas9 and mLP-CRISPR, did not provoke *IFNB1* expression in THP-1-derived macrophages and HEK293T cells, the latter is RNA-sensing functional but DNA-sensing dysfunctional (Fig. 3k and Supplementary Fig. 7a). By contrast, both in vitro-transcribed *Cas9* mRNA and in vitro-transcribed gRNA strongly induced a *IFNB1* response in HEK293T cells (Supplementary Fig. 7b,c). Accordingly, mLP-CRISPR treatment of HEK293T cells did not induce significant apoptosis at the dosage that we routinely used for efficient gene editing (Supplementary Fig. 8).

mLP-CRISPR targets RPE cells efficiently and specifically in vivo. To trace the spreading of treatment by subretinal injection, we injected 1.5 µl 0.2% sodium fluorescein and imaged the eye using a dissecting microscope 5 min later. We found nearly 100% fluorescence coverage of the retina, indicating that subretinal injection led to wide dissemination of the injected solution (Fig. 4a). As RPE cells are the primary source of VEGFA in the eyes, we next examined whether mLP-CRISPR has the ability to transduce the RPE cells specifically in vivo using confocal imaging (Fig. 4a). mLP-CRISPR was delivered by subretinal injection of the right eye, whereas the left eye was injected with PBS. mLP-CRISPR was visualized by staining for GFP, which was expressed from the same episomal lentiviral genome together with the gRNA. Notably, a single injection of 1.5 µl of mLP-CRISPR resulted in the transduction of almost the whole single-cell RPE layer specifically (Fig. 4b and Supplementary Fig. 9). The RPE specificity might result from the physical environment in the eye and from VSV-G tropism.

To characterize the biodistribution of mLP-CRISPR, we used qPCR to track the dissemination of episomal DNA components from mLP-CRISPR after subretinal delivery to the right eye (Fig. 4c). The RPE–choroid–scleral (RCS) complex of the right eye was transduced with on average 2 and 4 copies of the viral genome per diploid genome for *Vegfa*-targeting and scramble-targeting mLP-CRISPR, respectively ($n=4$ mice; $P=0.0139$ and $P<0.0001$, one-way analysis of variance (ANOVA); Fig. 4c). However, the number is higher in RPE cells, as they were the only transduced cell types. We next collected the liver, spleen and testes to analyse the whole-body dissemination of mLP-CRISPR. No above-background viral genome was detected in these organs for both the *Vegfa* and non-targeting (scramble) mLP-CRISPR ($n\geq5$ mice; non-significant, one-way ANOVA; Fig. 4d).

Taken together, mLP-CRISPR delivered by subretinal injection efficiently and specifically targets RPE cells, and the edits are restricted to the injected eyes.

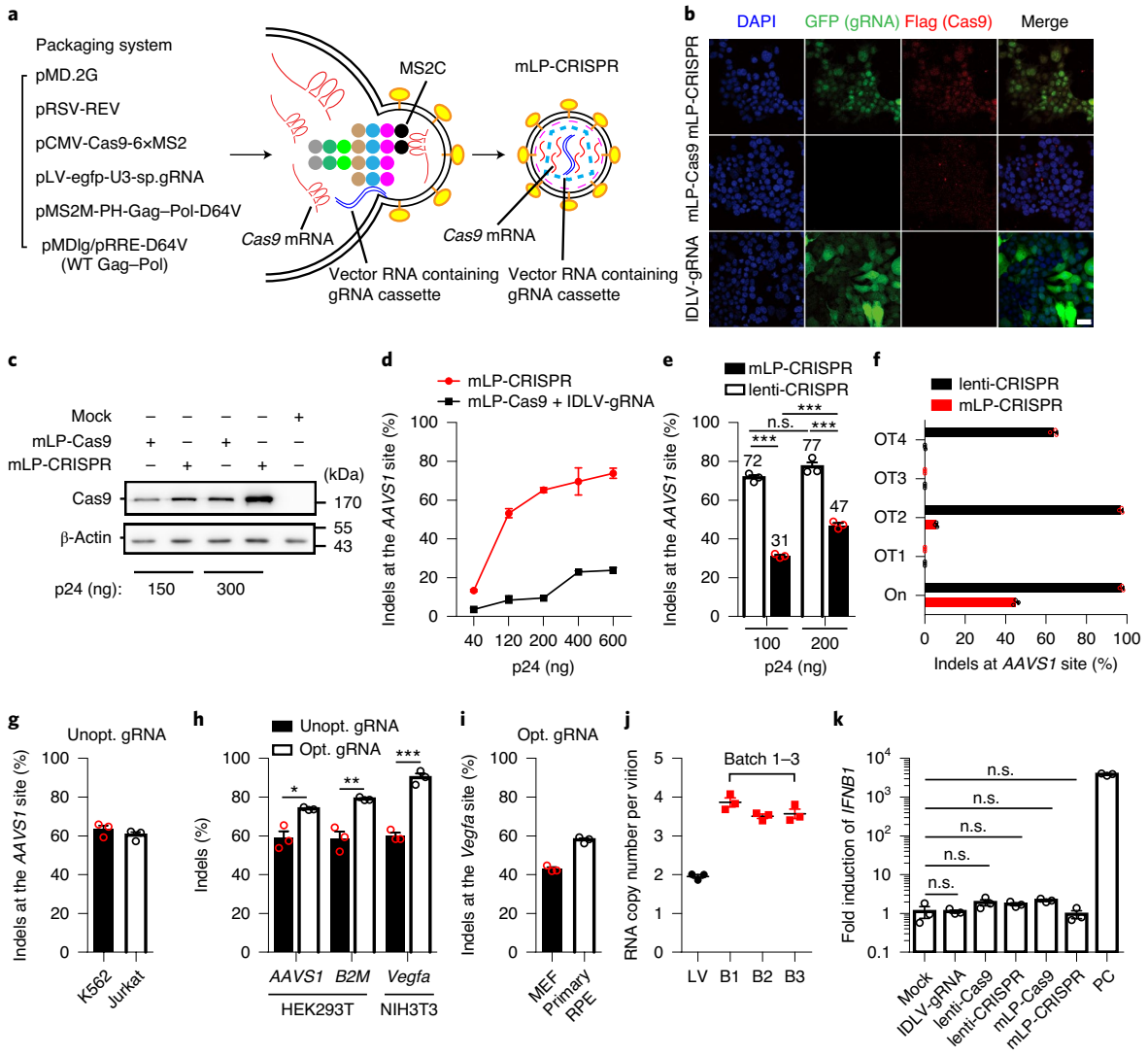

Fig. 3 | All-in-one mLP-CRISPR enhances gene-editing efficiency. a, The packaging system, and the process for producing the all-in-one mLP-CRISPR. **b**, Confocal microscopy analysis of the co-packaged *Cas9* mRNA and gRNA. GFP is indicative of the presence of gRNA, as they are in the same vector. Cas9 was visualized by staining its Flag tag. For each vector, 100 ng p24. Three images were taken for each group. Scale bar, 30 μm. **c**, Western blot analysis of Cas9 expression. Supplementing wild-type Gag–Pol (pMDlg/pRRE-D64V) during mLP-CRISPR production improved *Cas9* delivery compared with mLP-Cas9, for which production of wild-type Gag–Pol was not provided. **d**, Comparison of indel formation by the all-in-one mLP-CRISPR system and the split system (mLP-Cas9 + IDLV-gRNA) in HEK293T cells. **e**, Comparison of indel formation by mLP-CRISPR and lenti-CRISPR transduction in HEK293T cells. ***$P < 0.0001$ and $P = 0.0003$ (100 ng p24 and 200 ng p24 mLP-CRISPR versus lenti-CRISPR, respectively); ***$P = 0.0002$ (100 versus 200 ng p24 mLP-CRISPR). **f**, Deep-sequencing analysis of the off-target effects of mLP-CRISPR and lenti-CRISPR (200 ng p24) 15 d after infection. On, on target; OT, off target. **g**, Indel formation by mLP-CRISPR in K562 and Jurkat cells (300 ng p24). **h**, An optimized (Opt.) gRNA backbone enhanced the gene-editing efficiency of mLP-CRISPR in different cell types at various genomic loci (250 ng p24). *$P = 0.0126$ (*AAVS1*), **$P = 0.0051$ (*B2M*) and ***$P = 0.0003$ (*Vegfa*) for optimized versus unoptimized (Unopt.) gRNA. **i**, Gene editing by the *Vegfa*-targeting mLP-CRISPR with an optimized gRNA backbone in MEFs and primary RPE cells (250 ng p24). **j**, The copy number of mRNA in each mLP-CRISPR particle. B1, B2 and B3 represent different batches of mLP-CRISPR. LV, lenti-CRISPR. **k**, Induction of *IFNB1* in THP-1-derived macrophages by IDLV-gRNA, lenti-Cas9, lenti-CRISPR, mLP-Cas9 and mLP-CRISPR treatment. For each, 100 ng p24. For **d**–**i**, cells were seeded 24 h before transduction at a density of 2×10^4 per well. For **k**, THP-1 cells were seeded at a density of 1.5×10^5 per well in the presence of 150 nM phorbol 12-myristate 13-acetate (PMA) 48 h before transduction. PC, positive control. For **d**, **e**, **g**–**i**, indel frequency was determined using Sanger sequencing, and was analysed using TIDE. For **d**–**k**, data are mean ± s.e.m. from three biologically independent replicates. Statistical analysis was performed using unpaired two-tailed Student's *t*-tests.

In vivo knockout of *Vegfa* after a single injection of mLP-CRISPR. To examine the therapeutic potential of mLP-CRISPR, we delivered it subretinally, and then evaluated the gene-editing events and VEGFA expression (Fig. 5a). Seven days after subretinal injection, the RCS complex was dissected for analysis. We saw on average about 0.5% gene editing in the eyes that were treated with *Vegfa*-targeting mLP-CRISPR, significantly higher compared with in the PBS-injected control (Supplementary Fig. 10a). We reasoned that, because mLP specifically infected RPE cells, the low gene editing reflected the dilution by the choroid/scleral components. Indeed, we found that *Vegfa*-targeting mLP-CRISPR significantly decreased the overall VEGFA level in the RCS complex compared

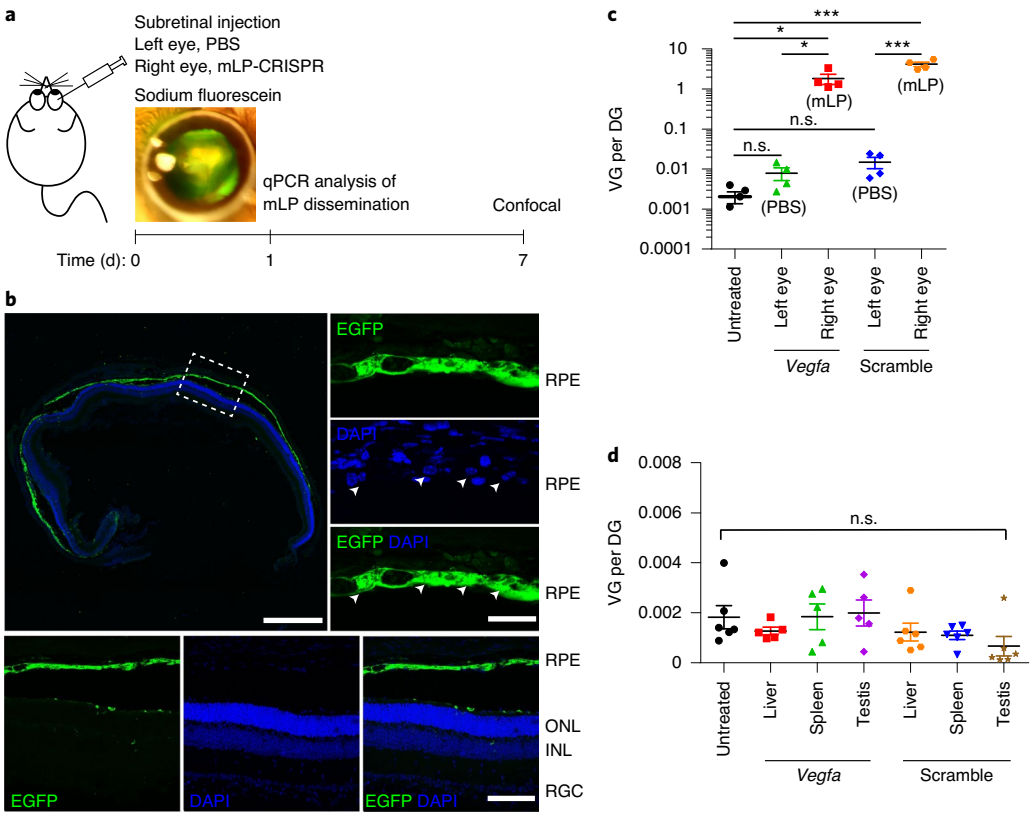

Fig. 4 | mLP-CRISPR targets RPE cells efficiently and specifically in vivo. a, Experimental workflow. Dissecting microscopy analysis of the eyeball 5 min after injection of 0.2% sodium fluorescein to verify successful subretinal injection. **b**, Confocal imaging analysis of the localization of mLP-CRISPR in the eyes. The right and bottom images are magnified versions of the area indicated by the white box in the top left image. The white arrowheads indicate the location of RPE cells. ONL, outer nuclear layer; INL, inner nuclear layer; RGC, retinal ganglion cells. The experiment was repeated twice with similar results. Scale bars, 500 μm (top left), 100 μm (bottom right) and 30 μm (top right). **c**, qPCR quantification of mLP-CRISPR dissemination between two eyes shown as viral genomes (VG) per diploid genome (DG). $n=4$ mice. The RCS complex was dissected for analysis. RCS samples from untreated mice were used as controls. $^{*}P=0.0139$ (*Vegfa*, right eye versus left eye); $^{*}P=0.0136$ (*Vegfa*, right eye versus untreated); $^{***}P<0.0001$ (scramble, right versus left and untreated eyes). **d**, qPCR analysis of mLP-CRISPR dissemination in the liver, spleen and testes showed as viral genomes per diploid genome. $n=6$ mice (untreated and scramble); $n=5$ mice (*Vegfa*). Liver samples from untreated mice used as controls. For each mouse, 100 ng p24 of mLP was used. For **c** and **d**, data are mean ± s.e.m. Statistical analysis was performed using one-way ANOVA with Tukey's post hoc test.

with the non-targeting mLP-CRISPR. This suggests that actual gene editing should be much higher in RPE cells (Supplementary Fig. 10b,c).

To analyse gene editing in RPE cells, we dissected the single-cell RPE layers from six mice two weeks after injection of mLP-CRISPR, and pooled them together for subsequent deep-sequencing analysis. By doing this, we observed 13% indel formation in the pure RPE population (Fig. 5b). Furthermore, we scrutinized the off-targeting events by sequencing the top-seven predicted off-target sites. We did not detect indels at all of the examined loci (Fig. 5b). The indel profile revealed that the majority of mLP-CRISPR-induced mutations were deletions (Fig. 5c). We next evaluated the level of VEGFA in the RCS complex. In agreement with the one-week data, we found that *Vegfa*-targeting mLP-CRISPR significantly downregulated the VEGFA level two weeks after injection ($n=6$ mice; $P=0.0005$, Student's *t*-test), but not the non-targeting mLP-CRISPR (Fig. 5d,e).

Limiting the immune responses to gene therapy products is of fundamental importance to the success of gene therapy. We first determined the type-I IFN response. As with the in vitro study, we were not able to detect above-background induction of *Ifnb1* and interferon-stimulated gene 15 (*ISG15*) in the RCS complex 24 h after mLP-CRISPR delivery in vivo (Fig. 6a,b and Supplementary Fig. 11). Macrophages are involved in first-line immune responses against viral infections, and will initiate a strong *Ifnb1* response once they have sensed the infection, which was not the case here (Fig. 6a,b). It is therefore probable that macrophages do not have an important role in this case. It has been reported that *Cas9* delivery to mouse livers using adenoviral vectors and AAVs induces Cas9-specific cellular and humoral responses[51]. Although the eyes are generally considered to be immune-privileged organs, T-cell infiltration can still be observed under pathogenic conditions[52]. We therefore examined T-cell infiltration 7 d after subretinal injection of mLP-CRISPR. Notably, we did not find significantly more $CD3^{+}$ cells in the retinas and RPE layers ($n=4$ sections; non-significant, one-way ANOVA; Fig. 6c and Supplementary Fig. 12). We next examined whether the subretinal injection of mLP-CRISPR induces Cas9-specific IgG. Compared with the untreated group, we did not observe significantly higher Cas9-specific IgG generation for both *Vegfa*-targeting and non-targeting mLP-CRISPR ($n=5$ mice; non-significant, one-way ANOVA; Fig. 6d). Interestingly, when injected through the footpad route, mLP-CRISPR evoked a significant increase in anti-Cas9 IgG in the sera, suggesting that even transient *Cas9* exposure in dendritic-cell-enriched loci can induce humoral immune responses ($n=5$ mice; $P=0.0088$, one-way ANOVA; Fig. 6d).

In summary, our findings show that subretinal injection of mLP-CRISPR induces specific gene editing in vivo in RPE cells. This is achieved by transient nuclease exposure using *Cas9* mRNA,

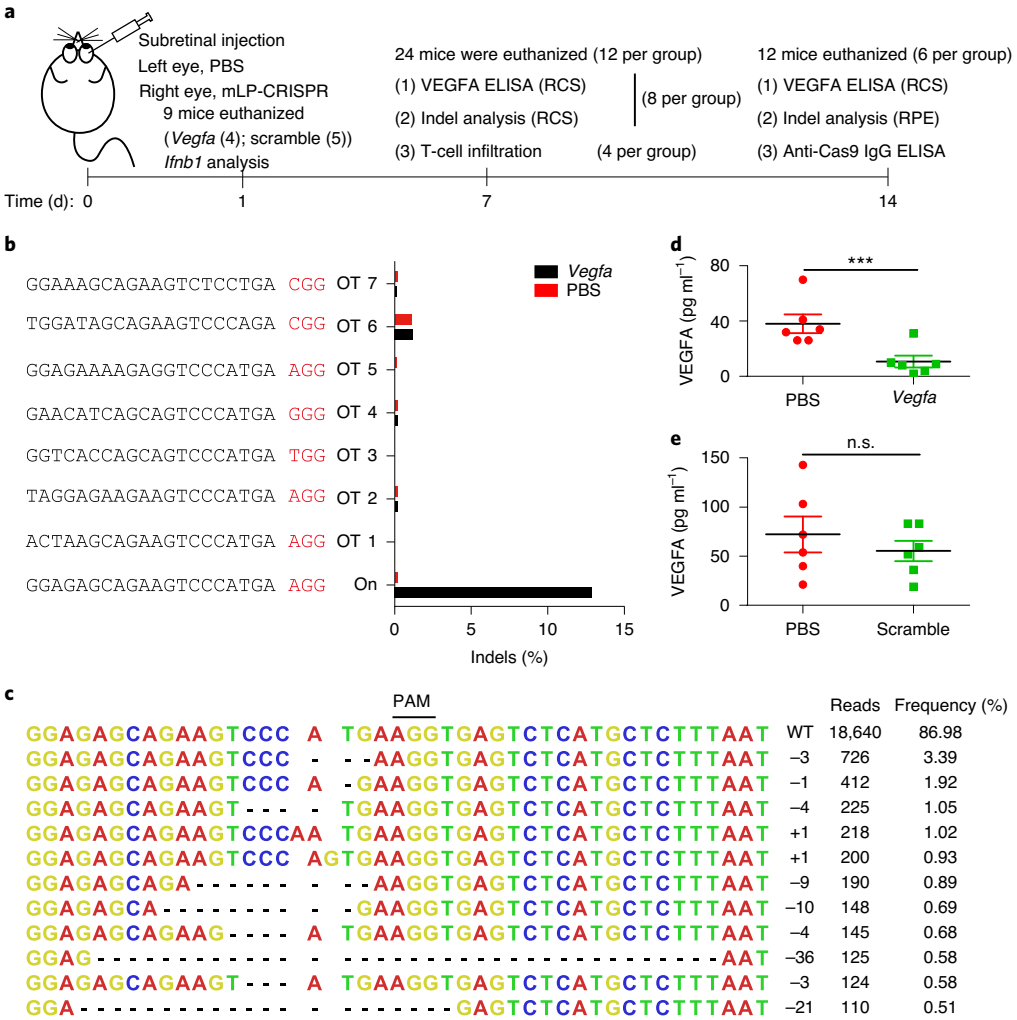

Fig. 5 | In vivo knockout of *Vegfa* after a single injection of mLP-CRISPR. a, Experimental workflow for Figs. 5 and 6. **b**, Deep-sequencing analysis of on-target (On) and off-target (OT) effects in pooled RPE cells dissected from six mice. Samples were collected two weeks after subretinal delivery of *Vegfa*-targeting mLP-CRISPR. **c**, The profile of mutations induced by *Vegfa*-targeting mLP-CRISPR. Frequencies of >0.1% were analysed and reads of >100 are shown. PAM, protospacer adjacent motif; WT, wild type. The minus symbol indicates a deletion and the plus symbol indicates an insertion. **d**,**e**, VEGFA levels in the RCS complex 14 d after injection of mLP-CRISPR. Only *Vegfa*-targeting (***$P = 0.0005$) (**d**) but not the non-targeting (**e**) mLP-CRISPR downregulated VEGFA. $n = 6$ mice. For each eye, 100 ng p24 of viral vector was used. For **d** and **e**, data are mean ± s.e.m. Statistical analysis was performed using paired two-tailed Student's *t*-tests.

without inducing significant innate and adaptive immune responses in the eyes.

mLP-CRISPR prevents CNV in a mouse model of laser-induced wAMD. To investigate the therapeutic efficacy of mLP-CRISPR, we used a laser-induced mouse model of wAMD. Furthermore, we adopted a 2× nuclear localization signal (NLS)-variant of Cas9, which contains two copies of the NLS. Using the 2× NLS Cas9, we showed improved efficiency compared with 1× NLS Cas9, which we had used in all previous experiments (Supplementary Fig. 13a). We also compared mLP-CRISPR that was packaged using a plasmid encoding 2× NLS *Cas9* mRNA fused with either a 6× or 12× MS2 stem loop, and found no significant difference regarding efficiency (Supplementary Fig. 13b). We therefore used 2× NLS and 6× MS2 stem loop Cas9 for the subsequent studies. We also chose a gRNA (designated *Vegfa* 2) that targets both the mouse and human *Vegfa* gene and was twice as efficient compared with the aforementioned *Vegfa* gRNA (Supplementary Fig. 14). In a pilot study, we performed a dose–response experiment, and we found that gene editing increased with the amount of mLP-CRISPR used (Supplementary Fig. 15). A schematic of the experiment protocol is shown in Fig. 7a. We first visualized the transduction and distribution of mLP-CRISPR in the RPE cells by staining the RPE layer with anti-GFP antibodies. We found that mLP-CRISPR transduced approximately two-thirds of the RPE cells (Fig. 7b). For humans, subretinal injections may cover only a small fraction of the surface area. In this case, direct single-loci injection to the location at which the lesion occurs or performing multiple-loci injections and optimizing the purity of the product may improve therapeutic efficacy. We next analysed on-target and off-target events using deep sequencing of the RPE genome pooled from six mice. The indel frequency of on-target *Vegfa* editing was 44%, whereas no off-target cutting was detected at four top-ranked off-target sites (Fig. 7c). Interestingly, we found that one specific mutation (1 bp insertion) was dominant (32.94%) in the indel profile induced by the *Vegfa*-targeting mLP-CRISPR (*Vegfa* 2; Fig. 7d). On-target large deletions induced by CRISPR have recently been reported in vitro[53]; these deletions were later confirmed in vivo using

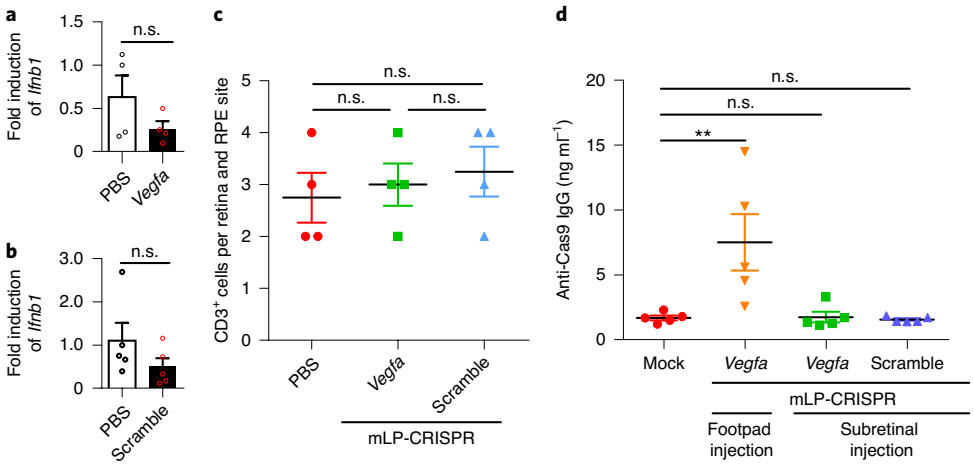

Fig. 6 | Immune responses to mLP-CRISPR. a,**b**, Fold induction of *Ifnb1* by *Vegfa*-targeting (**a**) and non-targeting (**b**) mLP-CRISPR in the RCS complex. For **a**, $n=4$ mice; for **b**, $n=5$ mice. **c**, Quantification of $CD3^+$ cells in retinas and the RPE layer 7 d after subretinal injection of mLP-CRISPR. $n=4$ histological sections. **d**, Anti-Cas9-specific IgG induction by subretinal injection of *Vegfa*-targeting and non-targeting mLP-CRISPR in the eyes. Footpad injection was used as a control. $n=5$ mice. $^{**}P=0.0088$ (footpad injection versus mock). For each eye, 100 ng p24 of viral vector was used. For **a**–**d**, data are mean ± s.e.m. Statistical analysis was performed using unpaired two-tailed Student's *t*-tests (**a** and **b**) and one-way ANOVA with Tukey's post hoc test (**c** and **d**).

AAV-delivered CRISPR, although at a low frequency (<0.5%)[11]. To detect potential large deletions induced by mLP-CRISPR, we performed Nanopore DNA-sequencing analysis of a 5.6-kb-long fragment across the cleavage site (Supplementary Figs. 16 and 17 and Supplementary Tables 4–6). Although we observed two large deletions, the frequencies (0.03% and 0.02%) were low and close to the detection limit of third-generation sequencing (Fig. 7e). We next measured VEGFA levels in the RCS tissues, and found that VEGFA in the mLP-CRISPR-treated group was reduced by 35% ($n=7$ mice; $P=0.0135$, Student's *t*-test; Fig. 7f). Importantly, we showed that *Vegfa*-targeting mLP-CRISPR treatment prevented CNV and significantly reduced the CNV area by 63% compared with the non-targeting counterpart ($n=21$–23 CNV areas; $P=0.0096$, Student's *t*-test; Fig. 7g,h). Although laser-induced CNVs have been shown to be variable, the model has been successful at predicting the clinical efficacy of anti-VEGF therapy for neovascular AMD if the correct criteria are followed[54]. Taken together, our results show that knocking out *Vegfa* in RPE cells using mLP-CRISPR significantly prevents the development of wAMD.

Discussion

Here we report a chimeric delivery system for the transient and efficient delivery of *Cas9*. In this system, *Cas9* is delivered as mRNA, and gRNA is expressed from reverse-transcribed viral DNA, which forms episomal circular DNA as the viral integrase is purposely mutated to avoid unwanted insertions[55]. Both *Cas9* mRNA and gRNA can be co-packaged into the same viral particle for efficient gene editing without inducing type-I IFN, which induces apoptosis and primes adaptive immune responses[56]. When applied in vivo, mLP-CRISPR transduces approximately two-thirds of the overall RPE cells but not the surrounding cell types. A single injection of mLP-CRISPR results in 13% and 44% *Vegfa* disruption in RPE cells with two different *Vegfa* gRNAs—*Vegfa* and *Vegfa* 2. The latter is human compatible and shows significant therapeutic efficacy in a mouse model of wAMD.

Direct sequencing of tissues would provide an unbiased analysis of off-target gene editing in vivo[57]. Common tools for the analysis of off-target edits can be divided into the following three types: (1) cell-based genome-wide assays, (2) in vitro genome-wide assays and (3) in silico prediction. They all have advantages and drawbacks. Cell-based methods can miss off-target mutations that occur with frequencies of lower than ~0.1%. Moreover, cell-based methods require high transfection efficiency, limiting its feasibility, scalability and reproducibility[58]. In vitro methods and their derivatives are more sensitive and comprehensive compared with cell-based methods, but their precision is compromised by chromatin accessibility, competition from endogenous DNA–protein binding and the concentration of genome-editing proteins in cells[57,59]. Here we used the in silico prediction tool CCTop, which is fast and relatively reliable[60]. We did not observe in vivo off-target edits for both gRNAs when we analysed the in silico-identified sites using deep sequencing. Although the analysis is not comprehensive, the fact that no off-target edits were found in most matched loci is reassuring.

It has been suspected that long-term suppression of VEGF is linked to the degeneration of retinal tissue[61]. However, direct evidence has not been established. A recent study showed that sustained suppression of VEGFA in non-human primates through the overexpression of aflibercept for more than 12 months does not change macular volume, macular thickness or retinal morphology[62]. Furthermore, a 12-month human study showed that repeated injections of ranibizumab did not alter the function of retinal ganglion cells[63]. Moreover, retinal degeneration and other adverse effects have not been reported in clinical trials of anti-VEGF gene therapy[64,65]. Further data from a variety of ongoing clinical trials testing multiple strategies, such as AAV expression of anti-VEGF antibodies to achieve sustained suppression of VEGF, may clarify the association[66]. The current data suggest that the benefits of long-term VEGF suppression far outweigh any risks[66].

In our study, we did not observe Cas9-specific immune responses after subretinal injection. In a recent study, delivery of Sa*Cas9* through the same route by AAV to non-human primates led to Cas9-specific IgG and T-cell responses in some of the animals, which suggests that the transient expression of *Cas9* may be less immunogenic[4]. However, we found Cas9-specific IgG for mLP injection in the animals' footpads, which are rich in antigen-presenting cells and are usually used for immunization. This should not be a surprise, as many vaccine technologies that are under development are based on short-lived mRNA and peptides[67]. The adaptive immune response to Cas9 is tissue-specific, and the administration of mLP-CRISPR to immunogenic organs should be carefully evaluated. Overall, it is

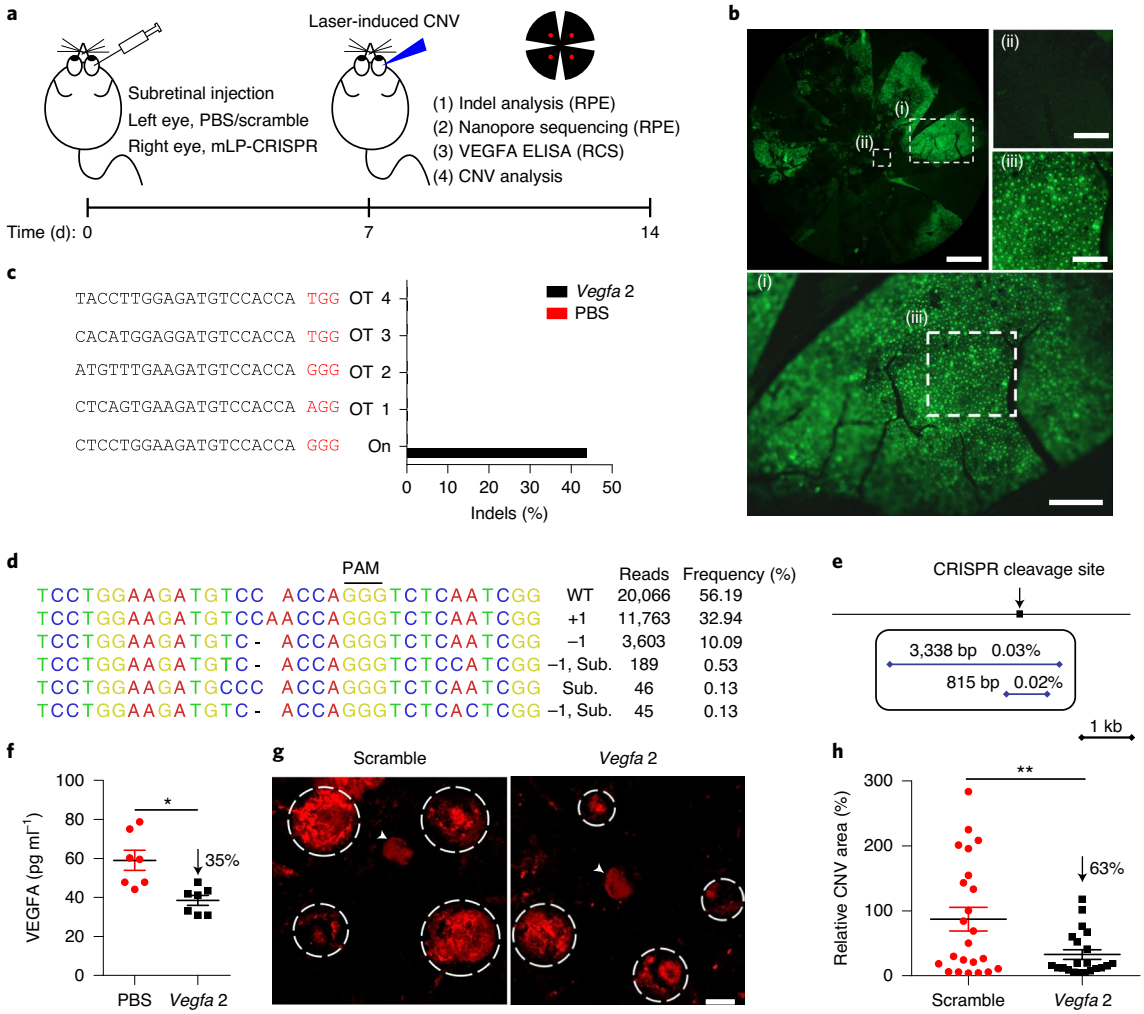

Fig. 7 | mLP-CRISPR prevents CNV in a mouse model of laser-induced wAMD. a, Experimental workflow. **b**, Fluorescence microscopy analysis of the distribution of mLP-CRISPR in the RPE layer 14 d after injection. GFP was expressed from mLP-CRISPR-infected RPE cells. The experiment was repeated twice with similar results. Magnifications of the areas indicated by white boxes are shown in the images with the corresponding labels (i–iii). Scale bars, 500 μm (top left), 200 μm (i) and 100 μm (ii and iii). **c**, Deep-sequencing analysis of the on-target (On) and off-target (OT) effects in pooled RPE cells at the *Vegfa* 2 target site dissected from six mice. Samples were collected two weeks after subretinal delivery of *Vegfa*-targeting mLP-CRISPR (*Vegfa* 2). **d**, The indel profile induced by *Vegfa*-targeting mLP-CRISPR (*Vegfa* 2). Frequencies of >0.1% were analysed. Sub., substitution. **e**, Nanopore DNA-sequencing analysis of large deletions in the RPE cells of a mouse treated with *Vegfa*-targeting mLP-CRISPR (*Vegfa* 2). $n=1$ mouse. The length and frequency of large deletions are indicated. **f**, Enzyme-linked immunosorbent assay (ELISA) analysis of VEGFA levels in the RCS complex 14 d after injection. $n=7$ mice. $^{*}P=0.0135$. **g**, Representative laser-induced CNVs stained with isolectin in the mouse eye injected with *Vegfa*-targeting mLP-CRISPR (*Vegfa* 2) or with the scrambled control. Six images were taken for each group. The white arrowheads indicate the position of the optic disc. Dashed white circles delineate CNVs. Scale bar, 200 μm. **h**, Analysis of the CNV areas from 6 mice 7 d after laser treatment. For each eye, 500 ng p24 of mLP was used. $n=23$ CNVs (scramble); $n=21$ CNVs (*Vegfa* 2). $^{**}P=0.0096$. For **f** and **h**, data are mean ± s.e.m. Statistical analysis was performed using a paired two-tailed Student's *t*-test (**f**) and an unpaired two-tailed Student's *t*-test with Welch's correction (**h**).

possible that human gene therapies using transient Cas9 exposure through mRNA delivery may evade the effects of pre-existing Cas9 immunity.

Outlook

In summary, we have developed a lentiviral system for efficient and safe gene editing in vivo. The system is suitable for CRISPR gene therapy in the eyes, owing to the absence of Cas9-specific immunity and the small therapeutic dose needed. Published results from clinical trials of wAMD gene therapy have shown the need for traditional anti-VEGF treatment (ranibizumab injection) to prevent disease progression, possibly due to the low expression of anti-VEGF inhibitor from AAVs (ref. [64]). In this regard, the efficacy and safety of mLP-CRISPR for in vivo gene therapy of wAMD is encouraging. Moreover, mLPs could be extended for the delivery of mRNA encoding base editors, epigenome editors and other types of gene-editing enzyme[68]. We also provide preliminary data showing that lentiviral particles can also deliver ABEmax, achieving an efficiency of more than 31% and 63% at two different loci[69] (Supplementary Fig. 18). For in vivo applications in large organs, in which a higher amount of mLP would be needed, the production yield of mLPs would need to be optimized.

Methods

Plasmid construction. pMS2M-PH-Gag–Pol-D64V and pMS2D-PH-Gag–Pol-D64V were constructed by replacing the *GFP* gene in the pGFP-PH-Gag–Pol-D64V

vector[23] with the AgeI- and AccIII-digested MS2C-encoding gene in the monomer form (MS2M) and dimer form (MS2D), respectively. pMDlg/pRRE-int-MS2M and pMDlg/pRRE-int-MS2D were constructed by inserting MS2M and MS2D into the C terminus of the insertion-defective integrase in the pMDlg/pRRE-D64V vector[23]. pCMV-GFP-3×MS2, pCMV-GFP-6×MS2, pCMV-GFP-12×MS2 and pCMV-Cas9-6×MS2 were generated by inserting MS2 stem loop repeats between the stop codon of the *GFP*/*Cas9* gene and the poly(A) sequence, while the whole expression cassette is under the control of CMV promoter. pLV-egfp-U3-sp.gRNA and pLV-egfp-U3-Osp.gRNA (containing the optimized gRNA backbone) were constructed by inserting the backbone of gRNA into the U3 region of the 3′ LTR into pCCL-PGK-egfp. The gRNAs were inserted into AarI-digested pLV-egfp-U3-sp.gRNA and pLV-egfp-U3-Osp.gRNA and BsmBI-digested LentiCRISPR v2 (ref. [48]). The gRNA sequences are provided in Supplementary Table 1. All of the plasmids used are available from Addgene.

Cell cultures. HEK293T cells, MEFs, NIH3T3 cells and primary RPE cells were cultured in DMEM (Gibco). K562, Jurkat and THP-1 cells were maintained in RPMI 1640 medium (Gibco). To boost cytokine production, THP-1 cells were differentiated into macrophage-like cells with 150 nM PMA (Sigma-Aldrich) before the experiment. The medium was supplemented with 10% fetal bovine serum, 2 mM L-glutamine (Gibco), 100 U ml^{-1} penicillin and 100 μg ml^{-1} streptomycin (Gibco). All cells were cultured at 37 °C under 5% (v/v) CO_2.

Production of mLP and lentivirus. HEK293T cells were seeded in 15 cm dishes at a density of 10^7 cells per dish 24 h before calcium phosphate transfection. Then, 24 h after transfection, the medium was refreshed, and the supernatants were collected 48 h and 72 h after transfection before passing through a filter (0.45 μm; Millipore) and ultracentrifugation at 25,000 r.p.m. at 4 °C for 2 h. Pellets were resuspended in PBS and stored at −80 °C. To produce mLP-GFP carrying *GFP* mRNA, the following plasmids were used: 9.07 μg pMD.2G, 7.26 μg pRSV-REV, 31.46 μg pMDlg/pRRE-int-MS2M (or 31.46 μg pMDlg/pRRE-int-MS2D) and 31.46 μg pCMV-GFP-6×MS2, or 9.07 μg pMD.2G, 31.46 μg pMS2M-PH-Gag–Pol-D64V (or 31.46 μg pMS2D-PH-Gag–Pol-D64V) and 31.46 μg pCMV-GFP-6×MS2. To produce mLP-Cas9, 9.07 μg pMD.2G, 31.46 μg pMS2M-PH-Gag–Pol-D64V and 31.46 μg pCMV-Cas9-6×MS2 were used. To produce lenti-Cas9, 9.07 μg pMD.2G, 7.26 μg pRSV-REV, 31.46 μg pMDlg/pRRE and 31.46 μg lentiCas9-Blast[48] were used for transfection. IDLV-gRNA (or IDLV) was produced using the following combination: 9.07 μg pMD.2G, 7.26 μg pRSV-REV, 31.46 μg pMDlg/pRRE-D64V and 31.46 μg pLV-egfp-U3-gRNA with the corresponding gRNA sequence (or 31.46 μg pCCL-PGK-egfp). To produce the all-in-one mLP, HEK293T cells were transfected with 9.07 μg pMD.2G, 7.26 μg pRSV-REV, 15.74 μg pMDlg/pRRE-D64V, 15.74 μg pMS2M-PH-Gag–Pol-D64V, 31.46 μg pCMV-Cas9-6×MS2 and 31.46 μg pLV-egfp-U3-gRNA with the corresponding gRNA sequence. To produce the all-in-one lenti-CRISPR, HEK293T cells were transfected with 9.07 μg pMD.2G, 7.26 μg pRSV-REV, 31.46 μg pMDlg/pRRE and lentiCRISPRv2-AAVS1.

TEM analysis. TEM was conducted using a 120 kV biology transmission electron microscope (Tecnai G2 spirit Biotwin) at the electron microscope laboratory at Shanghai Jiao Tong University. The samples were prepared on copper TEM grids (3.05 mm; 200 mesh) by negative staining. Then, 10 μl of each sample was pipetted onto copper TEM grids and incubated for 1–3 min. Uranyl acetate (10 μl, 2%) was pipetted onto the grids and incubated for 10 min. Excess solution was removed by blotting the grids at a 45° angle once from the side of the grid with filter paper. The sample was allowed to dry before observation under a Tecnai G2 Spirit Biotwin 120 kV TEM. Data were digitally recorded using a 150–250 k magnification CCD Gatan 832 camera.

Flow cytometry analysis. HEK293T cells were seeded onto a 24-well plate at a density of 4×10^4 per well 24 h before transduction with mLP that was produced by different packaging systems carrying *GFP* mRNA. Then, 72 h after transduction, the GFP signals were determined using flow cytometry (BD & LSR Fortessa). To analyse apoptosis induced by mLP, HEK293T cells were collected 60 h after transduction and double-stained with annexin V and propidium iodide using the Annexin V-PI apoptosis detection kit (Vazyme Biotech) according to the manufacturer's instructions. To determine the titre of lentivirus, HEK293T cells were seeded on the six-well plates at a density of 1×10^5 per well 24 h before transduction with different dilutions of IDLV. GFP signals were detected 72 h after transduction. Dilutions yielding 10% to 30% GFP^+ cells were used for titre calculations. The flow data were collected using BD FACSDiva v.7 and analysed using FlowJo v.7.6. The gating strategies are shown in Supplementary Fig. 19.

Western blotting. To detect epigenetic modification of lenti-Cas9 in HEK293T cells, the medium was supplied with/without histone deacetylase inhibitor trichostatin A (Targetmol) at a final concentration of 4 μM and 8 μM for 18 h during lenti-Cas9 transduction. For all of the western blotting experiments, cells and mLP particles were lysed in RIPA in the presence of a protease inhibitor (Beyotime Biotechnology). The proteins were separated using SDS–polyacrylamide gel electrophoresis and transferred to a polyvinylidene difluoride membrane. The membranes were blocked by 5% fat-free milk dissolved in TBS/0.05% Tween-20 for 1 h, and incubated with anti-Cas9 monoclonal antibodies (1:3,000, Cell Signaling Technology) overnight at 4 °C. The membranes were incubated with anti-mouse secondary antibodies (1:3,000, Cell Signaling Technology) and visualized using LumiBest enhanced chemiluminescence (Shanghai Share-bio Biotechnology). β-actin detected using anti-β-actin monoclonal antibodies (1:3,000, Cell Signaling Technology) and p24 detected using anti-HIV-1 p24 monoclonal antibodies (1:1,000, Santa Cruz Biotechnology) were used for normalization across samples.

Mice. The animal experiments were performed at Shanghai Jiao Tong University and the Institute of Neuroscience, Shanghai Institutes for Biological Sciences, Chinese Academy of Sciences (CAS). The care, use and treatment of all of the animals in this study complied with the guidelines of the Institutional Animal Care and Use Committee (IACUC) of the Shanghai Jiao Tong University and the Biomedical Research Ethics Committee of the Shanghai Institutes for Biological Science, CAS. Pathogen-free C57BL/6J male mice (aged 8 weeks, 22 ± 1 g) were used in this study. Mice were housed in an environmentally controlled room (23 °C, with 55 ± 5% humidity and under a 12 h–12 h light–dark cycle). The all-in-one mLP-CRISPR or PBS was injected into mice by subretinal injection.

Laser-induced CNV model. Seven days after subretinal injection of mLP-CRISPR, mice were anaesthetized by 1.25% tribromoethanol. The pupils were dilated with phenylephrine (0.5%) and tropicamide (0.5%). CNV lesions were induced using a laser system (Visulas 532S, Carl Zeiss Meditec) with an intensity of 120 mW, wavelength of 532 nm, laser spot size of 50 μm and exposure time of 100 ms. Four laser burns were induced around each optic disc. Next, 7 d later, mice were sedated by pentobarbital sodium (25 mg kg^{-1}) before perfusion with 4% paraformaldehyde through the heart. The eyes were enucleated and fixed with 4% paraformaldehyde for 2 h. The RPE-choroid complex was incubated with blocking buffer (5% goat serum albumin (Beyotime Biotechnology) and 0.5% Triton X-100 (Solarbio) in PBS) for 1 h at 4 °C. RCS complexes were dissected for immunostaining and then incubated with AlexaFluor-594-conjugated isolectin (1:1,000; Vector Laboratories) overnight at 4 °C in blocking buffer. RCS complexes were flat-mounted and made into slices. The distribution of mLP-CRISPR in the RPE layer was analysed using a fluorescence microscope (Eclipse Ni, Nikon). CNVs were imaged using a fluorescent microscope (Olympus BX53). The CNV areas were measured using Image J with an established and constant threshold in pixels. Only burns that produced a bubble without haemorrhage were used for analysis. Outlier lesions that were more than 5× larger than the mean area of the other lesions in the same eye were excluded[54].

ELISA. The p24 of mLP and lentiviral particles was measured using HIV p24 ELISA according to the manufacturer's instructions (Beijing Biodragon Immunotechnologies). To detect total VEGFA protein levels, total protein of RCS was extracted using Trizol and diluted in 100 μl double-distilled H_2O. Samples were measured using a Mouse VEGFA ELISA Kit (Elabscience) according to the manufacturer's instructions. Humoral IgG immune response to Cas9 was measured using IgG Mouse ELISA Kit (Abcam) according to the manufacturer's protocol with a few modifications. A total of 0.25 μg of recombinant Cas9 proteins suspended in PBS was used to coat 96-well ELISA plates and incubated at 4 °C for 12 h. The wells were washed three times using 1× wash buffer. Plates were blocked with 2% bovine serum albumin blocking solution for 2 h at room temperature, then washed three times. Serum samples were diluted 1:2 using PBS and added to each well in duplicate. The remaining steps were performed according to the manufacturer's protocol. Anti-Cas9 mouse monoclonal antibodies (Cell Signaling Technology) were diluted according to the instructions of the IgG Mouse ELISA Kit to make a standard curve.

qPCR. Total RNA was extracted using RNAiso Plus (Takara), and cDNA was synthesized using the QuantScript RT Kit (TIANGEN) according to the manufacturer's protocol. THP-1 cells were induced for 48 h before transduction with 150 nM PMA. Then, 2 μg poly(I:C) was transfected using Lipofectamine 2000 (Thermo Fisher Scientific) as a positive control. The *IFNB1* in THP-1 cells was amplified using PowerUp SYBR Green Master Mix with the primers SK53/SK54 and normalized to *GAPDH* (SK55/SK56). The *IFNB1* in HEK293T cells and RCS samples was amplified using the TaqMan Fast Advanced Master Mix (Applied Biosystems) on the StepOnePlus Real-Time PCR system and normalized to *ACTB*. The TaqMan gene expression assays for HEK293T cells were *IFNB1* (Hs01077958_s1) and *ACTB* (Hs00357333_g1). The TaqMan gene expression assays used for in vivo experimentation were *IFNB1* (Mm00439552_s1) and *ACTB* (Mm01205647_g1). The gene expression of *ISG15* was detected using the PowerUp SYBR Green Master Mix with the primers SK51/SK52 and normalized to *GAPDH* (SK13/SK14). Copies of *Cas9* mRNA in the all-in-one mLP-CRISPR were quantified by comparing with the conventional lentiviral vector. RNAs extracted from the same p24 of mLP-CRISPR and lenti-CRISPR were synthesized to cDNA. RT–qPCR was performed using the PowerUp SYBR Green Master Mix (Applied Biosystems) according to the manufacturer's protocol using the primers SK11/SK12. Data of mLP-CRISPR were normalized to that of lenti-CRISPR. To detect mLP distribution in different organs, genomic DNA was extracted from

the eye, liver, spleen and testes using the Blood & Cell & Tissue Genomic DNA Kit (TIANGEN). qPCR was performed using the PowerUp SYBR Green Master Mix to detect *WPRE* (primer SK9/SK10) which was then normalized to *GAPDH* (SK13/SK14). A list of the primer sequences used is provided in Supplementary Table 2. For all the innate immune sensing experiments, RNAs were collected from THP-1 or HEK293T cells 6 h after transfection or transduction. The StepOnePlus Real-Time PCR system was used for the PCR experiment, and StepOne v.2.2.2 was used for data collection.

Deep-sequencing and TIDE analysis. The top-four predicted off-target sites for *AAVS1*-targeting gRNA, top-seven predicted off-target sites for *Vegfa* gRNA and top-four predicted off-target sites for *Vegfa* 2 gRNA were identified using the CCTop-CRISPR/Cas9 target online predictor. The on-target and predicted off-target regions were amplified according to the Hi-TOM Gene Editing Detection Kit (Novogene). The purified PCR products were pooled at an equal molar ratio for double-end sequencing using Illumina MiSeq at Novogene. Raw data of next-generation sequencing were analysed using Cas-analyzer[70]. A list of the primer sequences used is provided in Supplementary Table 3. For indel frequency analysis by TIDE, the purified PCR amplicons were Sanger-sequenced and decomposed using TIDE (v.2.0.1)[71]. To detect the frequency of base editing, the purified PCR amplicons were Sanger-sequenced and analysed using EditR (v.1.0.9)[72]. A list of the primers used is provided in Supplementary Table 1.

Immunofluorescence staining and imaging of cells and tissue. To verify the presence of *Cas9* mRNA and gRNA, HEK293T cells were seeded onto a 12-well plate containing coverglasses at a density of 6×10^4 cells per well 24 h before transduction with the all-in-one vector mLP-CRISPR, mLP-Cas9, IDLV-gRNA and lenti-CRISPR. Cells were fixed using 4% paraformaldehyde and stained with anti-Flag-tag antibodies (1:800, Proteintech) or anti-Cas9 monoclonal antibodies (1:800, Cell Signaling Technology) followed by Alexa Fluor 555 IgG (1:800, Cell Signaling Technology). The nuclei were stained with DAPI (Beyotime Biotechnology). The imaging was performed using a confocal microscope (A1si, Nikon). To localize the dissemination of mLP-CRISPR and quantify T-cell infiltration in the eyes, paraformaldehyde-fixed cryostat section samples were prepared 7 d after subretinal injection. Cross-section samples were stained with anti-GFP antibodies (1:1,500, Thermo Fisher Scientific) and anti-CD3 antibodies (1:100, GeneTex) followed by Alexa Fluor 488 IgG (1:500, Jackson ImmunoResearch) or Cy3 AffiniPure IgG (1:500, Jackson ImmunoResearch). The nuclei were stained by DAPI (Sigma-Aldrich) and mounted with SlowFade Diamond Antifade Mountant (Life Technologies) on glass slides. The imaging was performed using a confocal microscope (TiE-A1 plus, Nikon).

RPE cell isolation. After euthanizing the mice, the eyes were enucleated and immediately placed in precooled PBS. After clearing the tissue around and cutting the optic nerve under a dissecting microscope, the eye was incised with scissors behind the limbus, while the corneas, irises and lens were discarded. Vitreous body and retina were carefully removed. The eyecup (RCS tissue) was cut with 4–6 small slits from the peripheral edges to the optic nerve. The resultant tissue was flattened and incubated in a 1.5 ml Eppendorf tube containing 200 µl TrypLE (Gibco) at 37 °C for 5 min. The eyecup was tapped 50 times gently and quickly. The RPE cells were collected by centrifugation at 300*g*, 4 °C for 5 min after removing the choroid/scleral tissue. The RPE cells were washed with PBS three times.

Nanopore DNA sequencing and analysis. To detect potential large deletions induced by mLP-CRISPR in vivo, RPE cells were isolated 14 d after injection with *Vegfa*-targeting mLP-CRISPR (*Vegfa* 2). Before injection, a 5 mm tail piece was cut off as a blank control. Samples were lysed by QuickExtract (Epicentre) as PCR templates. A 5.6 kb PCR product across the CRISPR cut site was amplified by nested PCR (the first primers were SK61/SK62 and the second primers were SK63/SK64). Nanopore DNA sequencing was performed by Novogene using the PromethION platform. Clean reads were mapped to the mouse reference genome (GRCm38/mm10) using Minimap2 (ref. [73]). Structural variations (variations of >50 bp) were analysed using Sniffles (v.1.0.10)[74] and filtered by mouse tail sequencing data. The frequency of large deletions was calculated as the ratio of the variation reads number to the number of overall reads overlapping with the mutated regions, which were counted using intersectBed in bedtools v.2.0 (ref. [75]). Information about the quality of sequencing data and a summary of large deletions are provided in Supplementary Tables 5 and 6.

Statistics. Data were analysed using GraphPad Prism 7. Data are presented as mean ± s.e.m. in all of the experiments ($n \geq 3$). Student's *t*-tests or one-way ANOVA were performed to determine the *P* values (95% confidence interval). The specific statistical method applied and descriptions of replicates are provided in the figure legends. The asterisks indicate statistical significance; unless otherwise specified, $^*P<0.05$, $^{**}P<0.01$, $^{***}P<0.001$; n.s., non-significant.

Reporting Summary. Further information on research design is available in the Nature Research Reporting Summary linked to this article.

Data availability

The main data supporting the results in this study are available within the paper and its Supplementary Information. Source data for the figures are available at Figshare (https://doi.org/10.6084/m9.figshare.12611819)[76]. The deep-sequencing and Nanopore DNA-sequencing data are available at the NCBI BioProject under the identifiers PRJNA642029, PRJNA593168 and PRJNA628164.

Received: 3 December 2019; Accepted: 3 November 2020;
Published online: 04 January 2021

References

1. Dever, D. P. et al. CRISPR/Cas9 β-globin gene targeting in human haematopoietic stem cells. *Nature* **539**, 384–389 (2016).
2. Kim, K. et al. Genome surgery using Cas9 ribonucleoproteins for the treatment of age-related macular degeneration. *Genome Res.* **27**, 419–426 (2017).
3. van Diemen, F. R. et al. CRISPR/Cas9-mediated genome editing of herpesviruses limits productive and latent infections. *PLoS Pathog.* **12**, e1005701 (2016).
4. Maeder, M. L. et al. Development of a gene-editing approach to restore vision loss in Leber congenital amaurosis type 10. *Nat. Med.* **25**, 229–233 (2019).
5. Beyret, E. et al. Single-dose CRISPR-Cas9 therapy extends lifespan of mice with Hutchinson–Gilford progeria syndrome. *Nat. Med.* **25**, 419–422 (2019).
6. Santiago-Fernandez, O. et al. Development of a CRISPR/Cas9-based therapy for Hutchinson–Gilford progeria syndrome. *Nat. Med.* **25**, 423–426 (2019).
7. Kim, E. et al. In vivo genome editing with a small Cas9 orthologue derived from *Campylobacter jejuni*. *Nat. Commun.* **8**, 14500 (2017).
8. Li, A. et al. A self-deleting AAV-CRISPR system for in vivo genome editing. *Mol. Ther. Methods Clin. Dev.* **12**, 111–122 (2019).
9. Chew, W. L. et al. A multifunctional AAV-CRISPR-Cas9 and its host response. *Nat. Methods* **13**, 868–874 (2016).
10. Mingozzi, F. et al. Overcoming preexisting humoral immunity to AAV using capsid decoys. *Sci. Transl. Med.* **5**, 194ra192 (2013).
11. Nelson, C. E. et al. Long-term evaluation of AAV-CRISPR genome editing for Duchenne muscular dystrophy. *Nat. Med.* **25**, 427–432 (2019).
12. Wagner, D. L. et al. High prevalence of *Streptococcus pyogenes* Cas9-reactive T cells within the adult human population. *Nat. Med.* **25**, 242–248 (2019).
13. Wignakumar, T. & Fairchild, P. J. Evasion of pre-existing immunity to Cas9: a prerequisite for successful genome editing in vivo? *Curr. Transplant. Rep.* **6**, 127–133 (2019).
14. Gao, X. et al. Treatment of autosomal dominant hearing loss by in vivo delivery of genome editing agents. *Nature* **553**, 217–221 (2018).
15. Montagna, C. et al. VSV-G-enveloped vesicles for traceless delivery of CRISPR-Cas9. *Mol. Ther. Nucleic Acids* **12**, 453–462 (2018).
16. Lee, K. et al. Nanoparticle delivery of Cas9 ribonucleoprotein and donor DNA in vivo induces homology-directed DNA repair. *Nat. Biomed. Eng.* **1**, 889–901 (2017).
17. Lee, B. et al. Nanoparticle delivery of CRISPR into the brain rescues a mouse model of fragile X syndrome from exaggerated repetitive behaviours. *Nat. Biomed. Eng.* **2**, 497–507 (2018).
18. Shahbazi, R. et al. Targeted homology-directed repair in blood stem and progenitor cells with CRISPR nanoformulations. *Nat. Mater.* **18**, 1124–1132 (2019).
19. Alkilany, A. M. & Murphy, C. J. Toxicity and cellular uptake of gold nanoparticles: what we have learned so far? *J. Nanopart. Res.* **12**, 2313–2333 (2010).
20. Perry B Hackett, N. V. S. Gene therapy: delivering the second revolution in site-specific nucleases. *eLife* **3**, e02904 (2014).
21. Cai, Y. & Mikkelsen, J. G. Lentiviral delivery of proteins for genome engineering. *Curr. Gene Ther.* **16**, 194–206 (2016).
22. Naldini, L., Trono, D. & Verma, I. M. Lentiviral vectors, two decades later. *Science* **353**, 1101–1102 (2016).
23. Cai, Y., Bak, R. O. & Mikkelsen, J. G. Targeted genome editing by lentiviral protein transduction of zinc-finger and TAL-effector nucleases. *eLife* **3**, e01911 (2014).
24. Cai, Y. et al. DNA transposition by protein transduction of the PiggyBac transposase from lentiviral Gag precursors. *Nucleic Acids Res.* **42**, e28 (2014).
25. Choi, J. G. et al. Lentivirus pre-packed with Cas9 protein for safer gene editing. *Gene Ther.* **23**, 627–633 (2016).
26. Lu, B. et al. Delivering Sa*Cas9* mRNA by lentivirus-like bionanoparticles for transient expression and efficient genome editing. *Nucleic Acids Res.* **47**, e44 (2019).
27. Lyu, P., Javidi-Parsijani, P., Atala, A. & Lu, B. Delivering Cas9/sgRNA ribonucleoprotein (RNP) by lentiviral capsid-based bionanoparticles for efficient 'hit-and-run' genome editing. *Nucleic Acids Res.* **47**, e99 (2019).
28. Voelkel, C. et al. Protein transduction from retroviral Gag precursors. *Proc. Natl Acad. Sci. USA* **107**, 7805–7810 (2010).

29. Prel, A. et al. Highly efficient in vitro and in vivo delivery of functional RNAs using new versatile MS2-chimeric retrovirus-like particles. *Mol. Ther. Methods Clin. Dev.* **2**, 15039 (2015).
30. Mangeot, P. E. et al. Genome editing in primary cells and in vivo using viral-derived nanoblades loaded with Cas9-sgRNA ribonucleoproteins. *Nat. Commun.* **10**, 45 (2019).
31. Lim, L. S., Mitchell, P., Seddon, J. M., Holz, F. G. & Wong, T. Y. Age-related macular degeneration. *Lancet* **379**, 1728–1738 (2012).
32. Andreoli, C. M. & Miller, J. W. Anti-vascular endothelial growth factor therapy for ocular neovascular disease. *Curr. Opin. Ophthalmol.* **18**, 502–508 (2007).
33. Usui-Ouchi, A. & Friedlander, M. Anti-VEGF therapy: higher potency and long-lasting antagonism are not necessarily better. *J. Clin. Invest.* **129**, 3032–3034 (2019).
34. Campochiaro, P. A. et al. Lentiviral vector gene transfer of endostatin/angiostatin for macular degeneration (GEM) study. *Hum. Gene Ther.* **28**, 99–111 (2017).
35. Hughes, C. P. et al. AAV2/8 anti-angiogenic gene therapy using single-chain antibodies inhibits murine choroidal neovascularization. *Mol. Ther. Methods Clin. Dev.* **13**, 86–98 (2019).
36. Murakami, Y. et al. Inhibition of choroidal neovascularization via brief subretinal exposure to a newly developed lentiviral vector pseudotyped with sendai viral envelope proteins. *Hum. Gene Ther.* **21**, 199–209 (2009).
37. Ortinski, P. I., O'Donovan, B., Dong, X. & Kantor, B. Integrase-deficient lentiviral vector as an all-in-one platform for highly efficient CRISPR/Cas9-mediated gene editing. *Mol. Ther. Methods Clin. Dev.* **5**, 153–164 (2017).
38. Sürün, D. et al. High efficiency gene correction in hematopoietic cells by donor-template-free CRISPR/Cas9 genome editing. *Mol. Ther. Nucleic Acids* **10**, 1–8 (2018).
39. Holmgaard, A. et al. In vivo knockout of the *Vegfa* gene by lentiviral delivery of CRISPR/Cas9 in mouse retinal pigment epithelium cells. *Mol. Ther. Nucleic Acids* **9**, 89–99 (2017).
40. Koo, T. et al. CRISPR-LbCpf1 prevents choroidal neovascularization in a mouse model of age-related macular degeneration. *Nat. Commun.* **9**, 1855 (2018).
41. Saint-Geniez, M., Maldonado, A. E. & D'Amore, P. A. VEGF expression and receptor activation in the choroid during development and in the adult. *Invest. Ophthalmol. Vis. Sci.* **47**, 3135–3142 (2006).
42. Kuzembayeva, M., Dilley, K., Sardo, L. & Hu, W. S. Life of psi: how full-length HIV-1 RNAs become packaged genomes in the viral particles. *Virology* **454–455**, 362–370 (2014).
43. Pickett, G. G. & Peabody, D. S. Encapsidation of heterologous RNAs by bacteriophage MS2 coat protein. *Nucleic Acids Res.* **21**, 4621–4626 (1993).
44. Cai, Y. & Mikkelsen, J. G. Driving DNA transposition by lentiviral protein transduction. *Mob. Genet. Elem.* **4**, e29591 (2014).
45. Skipper, K. A. et al. Time-restricted PiggyBac DNA transposition by transposase protein delivery using lentivirus-derived nanoparticles. *Mol. Ther. Nucleic Acids* **11**, 253–262 (2018).
46. Ihry, R. J. et al. p53 inhibits CRISPR–Cas9 engineering in human pluripotent stem cells. *Nat. Med.* **24**, 939–946 (2018).
47. Ellis, J. Silencing and variegation of gammaretrovirus and lentivirus vectors. *Hum. Gene Ther.* **16**, 1241–1246 (2005).
48. Sanjana, N. E., Shalem, O. & Zhang, F. Improved vectors and genome-wide libraries for CRISPR screening. *Nat. Methods* **11**, 783–784 (2014).
49. Kim, S., Kim, D., Cho, S. W., Kim, J. & Kim, J. S. Highly efficient RNA-guided genome editing in human cells via delivery of purified Cas9 ribonucleoproteins. *Genome Res.* **24**, 1012–1019 (2014).
50. Dang, Y. et al. Optimizing sgRNA structure to improve CRISPR-Cas9 knockout efficiency. *Genome Biol.* **16**, 280 (2015).
51. Wang, D. et al. Adenovirus-mediated somatic genome editing of *Pten* by CRISPR/Cas9 in mouse liver in spite of Cas9-Specific immune responses. *Hum. Gene Ther.* **26**, 432–442 (2015).
52. Zeka, B. et al. Aquaporin 4-specific T cells and NMO-IgG cause primary retinal damage in experimental NMO/SD. *Acta Neuropathol. Commun.* **4**, 82 (2016).
53. Kosicki, M., Tomberg, K. & Bradley, A. Repair of double-strand breaks induced by CRISPR–Cas9 leads to large deletions and complex rearrangements. *Nat. Biotechnol.* **36**, 765–771 (2018).
54. Gong, Y. et al. Optimization of an Image-guided laser-induced choroidal neovascularization model in mice. *PLoS ONE* **10**, e0132643 (2015).
55. Staunstrup, N. H. et al. Hybrid lentivirus-transposon vectors with a random integration profile in human cells. *Mol. Ther.* **17**, 1205–1214 (2009).
56. Paludan, S. R., Reinert, L. S. & Hornung, V. DNA-stimulated cell death: implications for host defence, inflammatory diseases and cancer. *Nat. Rev. Immunol.* **19**, 141–153 (2019).
57. Akcakaya, P. et al. In vivo CRISPR editing with no detectable genome-wide off-target mutations. *Nature* **561**, 416–419 (2018).
58. Tsai, S. Q. et al. GUIDE-seq enables genome-wide profiling of off-target cleavage by CRISPR–Cas nucleases. *Nat. Biotechnol.* **33**, 187–197 (2015).
59. Cheng, Y. & Tsai, S. Q. Illuminating the genome-wide activity of genome editors for safe and effective therapeutics. *Genome Biol.* **19**, 226 (2018).
60. Stemmer, M., Thumberger, T., del Sol Keyer, M., Wittbrodt, J. & Mateo, J. L. CCTop: an intuitive, flexible and reliable CRISPR/Cas9 target prediction tool. *PLoS ONE* **10**, e0124633 (2015).
61. Kurihara, T., Westenskow, P. D., Bravo, S., Aguilar, E. & Friedlander, M. Targeted deletion of *Vegfa* in adult mice induces vision loss. *J. Clin. Invest.* **122**, 4213–4217 (2012).
62. Grishanin, R. et al. Preclinical evaluation of ADVM-022, a novel gene therapy approach to treating wet age-related macular degeneration. *Mol. Ther.* **27**, 118–129 (2019).
63. Nishimura, T., Machida, S., Harada, T. & Kurosaka, D. Retinal ganglion cell function after repeated intravitreal injections of ranibizumab in patients with age-related macular degeneration. *Clin. Ophthalmol.* **6**, 1073–1082 (2012).
64. Rakoczy, E. P. et al. Three-year follow-up of phase 1 and 2a rAAV.sFLT-1 subretinal gene therapy trials for exudative age-related macular degeneration. *Am. J. Ophthalmol.* **204**, 113–123 (2019).
65. Rakoczy, E. P. et al. Gene therapy with recombinant adeno-associated vectors for neovascular age-related macular degeneration: 1 year follow-up of a phase 1 randomised clinical trial. *Lancet* **386**, 2395–2403 (2015).
66. Campochiaro, P. A. Low risk to retina from sustained suppression of VEGF. *J. Clin. Invest.* **129**, 3029–3031 (2019).
67. Richner, J. M. et al. Modified mRNA vaccines protect against Zika virus infection. *Cell* **168**, 1114–1125 (2017).
68. Thuronyi, B. W. et al. Continuous evolution of base editors with expanded target compatibility and improved activity. *Nat. Biotechnol.* **37**, 1070–1079 (2019).
69. Koblan, L. W. et al. Improving cytidine and adenine base editors by expression optimization and ancestral reconstruction. *Nat. Biotechnol.* **36**, 843–846 (2018).
70. Park, J., Lim, K., Kim, J. S. & Bae, S. Cas-analyzer: an online tool for assessing genome editing results using NGS data. *Bioinformatics* **33**, 286–288 (2017).
71. Brinkman, E. K., Chen, T., Amendola, M. & van Steensel, B. Easy quantitative assessment of genome editing by sequence trace decomposition. *Nucleic Acids Res.* **42**, e168 (2014).
72. Kluesner, M. G. et al. EditR: a method to quantify base editing from Sanger sequencing. *CRISPR J.* **1**, 239–250 (2018).
73. Li, H. Minimap2: pairwise alignment for nucleotide sequences. *Bioinformatics* **34**, 3094–3100 (2018).
74. Sedlazeck, F. J. et al. Accurate detection of complex structural variations using single-molecule sequencing. *Nat. Methods* **15**, 461–468 (2018).
75. Quinlan, A. R. & Hall, I. M. BEDTools: a flexible suite of utilities for comparing genomic features. *Bioinformatics* **26**, 841–842 (2010).
76. Ling, S. et al. Dataset for Lentiviral delivery of co-packaged *Cas9* mRNA and a *Vegfa*-targeting guide RNA prevents wet age-related macular degeneration in mice. *Fighare* https://doi.org/10.6084/m9.figshare.12611819 (2020).

Acknowledgements

We thank W. Yang at the Southern Medical University, China, for discussions and scientific input for the immunology part of the study. Y.C. is supported by the National Natural Science Foundation of China (no. 31971364), Pujiang Talent Project of Shanghai (no. 18PJ1404500), Shanghai Municipal Natural Science Foundation (no. 18ZR1419300), and startup funding from Shanghai Center for Systems Biomedicine, Shanghai Jiao Tong University (no. WF220441504).

Author contributions

S.L. and Y.C. conceived the study and designed the experiments; S.L., S.Y., X.H., D.Y., Y.D., X.Q., D.W. and J.H. performed the experiments; all of the authors analysed the data; S.L. and Y.C. wrote the manuscript with help from all of the authors.

Competing interests

The authors declare no competing interests.

Additional information

Supplementary information is available for this paper at https://doi.org/10.1038/s41551-020-00656-y.

Correspondence and requests for materials should be addressed to Y.C.

Reprints and permissions information is available at www.nature.com/reprints.

Publisher's note Springer Nature remains neutral with regard to jurisdictional claims in published maps and institutional affiliations.

nature research

Corresponding author(s): Yujia Cai

Last updated by author(s): Nov 3, 2020

Reporting Summary

Nature Research wishes to improve the reproducibility of the work that we publish. This form provides structure for consistency and transparency in reporting. For further information on Nature Research policies, see our Editorial Policies and the Editorial Policy Checklist.

Statistics

For all statistical analyses, confirm that the following items are present in the figure legend, table legend, main text, or Methods section.

n/a	Confirmed	
☐	☒	The exact sample size (*n*) for each experimental group/condition, given as a discrete number and unit of measurement
☐	☒	A statement on whether measurements were taken from distinct samples or whether the same sample was measured repeatedly
☐	☒	The statistical test(s) used AND whether they are one- or two-sided *Only common tests should be described solely by name; describe more complex techniques in the Methods section.*
☒	☐	A description of all covariates tested
☐	☒	A description of any assumptions or corrections, such as tests of normality and adjustment for multiple comparisons
☐	☒	A full description of the statistical parameters including central tendency (e.g. means) or other basic estimates (e.g. regression coefficient) AND variation (e.g. standard deviation) or associated estimates of uncertainty (e.g. confidence intervals)
☒	☐	For null hypothesis testing, the test statistic (e.g. *F*, *t*, *r*) with confidence intervals, effect sizes, degrees of freedom and *P* value noted *Give P values as exact values whenever suitable.*
☒	☐	For Bayesian analysis, information on the choice of priors and Markov chain Monte Carlo settings
☒	☐	For hierarchical and complex designs, identification of the appropriate level for tests and full reporting of outcomes
☒	☐	Estimates of effect sizes (e.g. Cohen's *d*, Pearson's *r*), indicating how they were calculated

Our web collection on statistics for biologists contains articles on many of the points above.

Software and code

Policy information about availability of computer code

Data collection	No customized software was used; BD FACSDiva 7 was used to collect flow-cytometry data; Applied Biosystems StepOnePlus Real-Time PCR system and StepOne 2.2.2 software were used to collect real-time PCR data; Fluorescence images were collected by using a fluorescence microscope (Eclipse Ni, Nikon and Olympus BX53) and a confocal microscope (A1si,Nikon and TiE-A1 plus, Nikon) with associated software. Western blot data were collected by the FlourChem E system.
Data analysis	GraphPad Prism 7, Cas-analyzer (version 2016.12.14), TIDE 2.0.1, EditR 1.0.9, (Fiji Is Just) ImageJ, FlowJo 7.6, Minimap2, Sniffles 1.0.10, bedtools 2.0.

For manuscripts utilizing custom algorithms or software that are central to the research but not yet described in published literature, software must be made available to editors and reviewers. We strongly encourage code deposition in a community repository (e.g. GitHub). See the Nature Research guidelines for submitting code & software for further information.

Data

Policy information about availability of data

All manuscripts must include a data availability statement. This statement should provide the following information, where applicable:

- Accession codes, unique identifiers, or web links for publicly available datasets
- A list of figures that have associated raw data
- A description of any restrictions on data availability

The main data supporting the results in this study are available within the paper and its Supplementary Information. Source data for the figures are available in figshare with the identifier doi: 10.6084/m9.figshare.1261181976. The deep-sequencing and nanopore-DNA sequencing data are available at the NCBI BioProject with the identifiers PRJNA642029, PRJNA593168 and PRJNA628164.

Field-specific reporting

Please select the one below that is the best fit for your research. If you are not sure, read the appropriate sections before making your selection.

☒ Life sciences ☐ Behavioural & social sciences ☐ Ecological, evolutionary & environmental sciences

For a reference copy of the document with all sections, see nature.com/documents/nr-reporting-summary-flat.pdf

Life sciences study design

All studies must disclose on these points even when the disclosure is negative.

Sample size	No sample-size calculations were performed to power each study. Generally, sample sizes were chosen to meet or exceed the standards of reproducibility demonstrated in similar published studies.
Data exclusions	In the analysis of areas of laser-induced choroidal neovascularization, only burns that produced a bubble without haemorrhage were used for analysis. Outlier lesions, with areas more than 5 times larger than the mean area of the other lesions in the same eye, were excluded.
Replication	Three biologically independent replicates were performed unless otherwise noted.
Randomization	For the in vitro experiments, samples were randomly allocated into experimental groups. For the in vivo studies, animals were randomly grouped.
Blinding	The investigators were not blinded.

Reporting for specific materials, systems and methods

We require information from authors about some types of materials, experimental systems and methods used in many studies. Here, indicate whether each material, system or method listed is relevant to your study. If you are not sure if a list item applies to your research, read the appropriate section before selecting a response.

Materials & experimental systems

n/a	Involved in the study
☐	☒ Antibodies
☐	☒ Eukaryotic cell lines
☒	☐ Palaeontology and archaeology
☐	☒ Animals and other organisms
☒	☐ Human research participants
☒	☐ Clinical data
☒	☐ Dual use research of concern

Methods

n/a	Involved in the study
☒	☐ ChIP-seq
☐	☒ Flow cytometry
☒	☐ MRI-based neuroimaging

Antibodies

Antibodies used	Antibodies used for western blotting: Cas9 (7A9-3A3) Mouse mAb (Cell Signaling Technology, 14697, Lot: 3),1:3000 β-Actin (8H10D10) Mouse mAb (Cell Signaling Technology, 3700, Lot: 15),1:3000 HIV-1 p24 mAb (Santa Cruz Biotechnology, sc-69728, Lot: F0717),1:1000 Anti-mouse IgG, HRP-linked Antibody (Cell Signaling Technology, 7076),1:3000 Antibodies used for immunofluorescence: FLAG® Antibody (Proteintech, 66008-3-Ig, Lot: 10010017),1:800 Cas9 (7A9-3A3) Mouse mAb (Cell Signaling Technology, 14697, Lot: 3),1:800 Alexa Fluor 555 IgG (Cell Signaling Technology, 4409,Lot:16),1:800 GFP Polyclonal antibody (ThermoFisher Scientific, A-6455),1:1500 Alexa Fluor 488 IgG AffiniPure Donkey Anti-Rabbit IgG (Jackson ImmunoResearch, 711-545-152),1:500 CD3 antibody [CD3-12] (GeneTex, GTX42110),1:100 Cy™3 AffiniPure Donkey Anti-Rat IgG (Jackson ImmunoResearch, 712-165-153),1:500 DyLight® 594 GSL I-B4 isolectin (Vector Laboratories, DL-1207-.5),1:1000 Antibodies used for ELISA anti-VEGFA was coated on the plate in VEGFA ELISA Kit (Elabscience, E-EL-M1292C, Lot: GLZL5YXRW9)
Validation	Antibodies were validated for each application by using the manufacturer's guidelines. Multiple dilutions were tested to determine the most appropriate dilution. Manufacturers released certificates of analysis for each lot used. Cas9 (7A9-3A3) Mouse mAb has been validated by western blot and immunofluorescence (https://www.cst-c.com.cn/products/

primary-antibodies/cas9-7a9-3a3-mouse-mab/14697).
β-Actin (8H10D10) Mouse mAb has been validated by western blot (https://www.cst-c.com.cn/products/primary-antibodies/b-actin-8h10d10-mouse-mab/3700).
HIV-1 p24 mAb has been validated by western blot (PMID: 30131116).
FLAG® Antibody has been validated by western blot and immunofluorescence (PMID: 30529465).
Alexa Fluor 555 IgG has been validated by immunofluorescence (PMID: 29203870).
GFP Polyclonal antibody has been validated by Immunostaining (PMID: 30158508).
CD3 antibody [CD3-12] has been validated by immunohistochemistry (PMID: 29603747) and immunofluorescence using T cell rich spleen tissue section in our laboratory.
DyLight® 594 GSL I-B4 isolectin has been validated by immunofluorescence (https://vectorlabs.com/dylight-594-labeled-gsl-i-isolectin-b4.html#biozbadges).

Eukaryotic cell lines

Policy information about cell lines

Cell line source(s)	K562, Jurkat, MEF and THP-1 cells were obtained from the laboratory of Soren Riis Paludan; 293T was obtained from the laboratory of Jacob G. Mikkelsen; NIH3T3 was obtained from the laboratory of Dali Li; primary RPE cells were freshly isolated from C57BL/6J mice. All the cell lines used in the study are from ATCC.
Authentication	None of the cell lines were authenticated.
Mycoplasma contamination	All cell lines tested negative for mycoplasma contamination.
Commonly misidentified lines (See ICLAC register)	No commonly misidentified cell lines were used.

Animals and other organisms

Policy information about studies involving animals; ARRIVE guidelines recommended for reporting animal research

Laboratory animals	Eight-week-old, male, 22 ± 1 grams, pathogen-free C57BL/6J mice were used. Mice were housed in an environmentally controlled room (23 °C, with 55 ± 5% humidity and 12 h / 12 h light–dark cycle).
Wild animals	The study did not involve wild animals.
Field-collected samples	The study did not involve samples collected from the field.
Ethics oversight	The animal experiments were performed at Shanghai Jiao Tong University and the Institute of Neuroscience, Shanghai Institutes for Biological Sciences, Chinese Academy of Sciences. The care, use, and treatment of all animals in this study have complied with the guidelines of the Institutional Animal Care and Use Committee (IACUC) of the Shanghai Jiao Tong University and the Biomedical Research Ethics Committee of the Shanghai Institutes for Biological Science, CAS.

Note that full information on the approval of the study protocol must also be provided in the manuscript.

Flow Cytometry

Plots

Confirm that:

☒ The axis labels state the marker and fluorochrome used (e.g. CD4-FITC).

☒ The axis scales are clearly visible. Include numbers along axes only for bottom left plot of group (a 'group' is an analysis of identical markers).

☒ All plots are contour plots with outliers or pseudocolor plots.

☒ A numerical value for number of cells or percentage (with statistics) is provided.

Methodology

Sample preparation	293T cells were harvested, washed with PBS for twice, and then fixed by 4% paraformaldehyde for 15 minutes at room temperature. After fixation, the cells were washed with PBS twice prior to analysis.
Instrument	LSR Fortessa flow cytometer (BD Biosciences).
Software	BD FACSDiva 7 was used to collect flow cytometry data; FlowJo 7.6 was used to analyse the data.
Cell population abundance	N/A
Gating strategy	293T cells were identified by forward and side scatter, followed by doublet exclusion. Cells were examined for GFP positivity. Non-transduced cells were used as a negative control to draw boundaries between GFP-positive and GFP-negative cells.

☒ Tick this box to confirm that a figure exemplifying the gating strategy is provided in the Supplementary Information.